A study of the threshold photoelectron spectra and the photoionisation yield curves of the boron trihalides

ARTICLE *in* CHEMICAL PHYSICS · MARCH 2003

Impact Factor: 1.65 · DOI: 10.1016/S0301-0104(03)00025-9 · Source: OAI

4 AUTHORS, INCLUDING:

David Shaw
Science and Technology Facilities Cou…

120 PUBLICATIONS **1,454** CITATIONS

Available online at www.sciencedirect.com
SCIENCE DIRECT®
Chemical Physics 288 (2003) 211–240
Chemical Physics
www.elsevier.com/locate/chemphys

A study of the threshold photoelectron spectra and the photoionisation yield curves of the boron trihalides

R.A. Mackie[a], L.G. Shpinkova[b], D.M.P. Holland[c,*], D.A. Shaw[c]

[a] Department of Pure and Applied Physics, The Queen's University of Belfast, Belfast, BT7 1NN, UK
[b] Department of Nuclear Spectroscopy Methods, Institute of Nuclear Physics, Moscow State University, Moscow 119899, Russia
[c] Daresbury Laboratory, Daresbury, Warrington, Cheshire, WA4 4AD, UK

Received 8 November 2002

Abstract

The valence shell threshold photoelectron spectra and the photoionisation yield curves of the boron trihalides have been recorded using synchrotron radiation. The threshold photoelectron spectra demonstrate that spin–orbit coupling is important in the heavier trihalides and affects the bands associated with degenerate orbitals. In addition to the photoelectron bands associated with direct ionisation, features have been observed due to autoionising Rydberg and valence excited states. An analysis of the vibrational progressions occurring in the photoelectron bands has enabled an almost complete set of ionic vibrational energies to be determined. The continuous nature of the inner valence shell photoelectron bands and the absence of main-lines illustrate the importance of electron correlation in redistributing the intensity amongst numerous final states. In all four of the boron trihalides, new Rydberg series have been observed in the photoionisation yield curves. However, prominent broad features attributable to intervalence transitions dominate the photoion spectra. In some Rydberg series the intensity distribution amongst the members appears irregular, and this may be due to mixing between Rydberg and valence excited states. Several, rather weak, vibrational progressions involving the v'_1, v'_2 and v'_4 modes have been observed.

1. Introduction

The inner-shell and core level photoabsorption spectra of the boron trihalides [1–6] provide some of the clearest examples of shape resonance phenomena affecting the photoionisation dynamics. Such spectra are characterised by a few strong and broad features, occurring both above and below the ionisation threshold, whilst the structure associated with Rydberg transitions is much less intense. This anomalous intensity distribution was originally discussed by Nefedov [7] and Dehmer [8]. A barrier, derived from the competition between repulsive centrifugal forces and attractive electrostatic forces, partitions the excited states into either the inner-well or the outer-well regions of the anisotropic molecular field. The virtual valence orbitals, located within the inner-well, overlap strongly with the core orbitals and this results

* Corresponding author. Tel.: +1925-603-425; fax: +1925-603-124.
E-mail address: d.m.p.holland@dl.ac.uk (D.M.P. Holland).

0301-0104/03/$ - see front matter © 2003 Elsevier Science B.V. All rights reserved.
doi:10.1016/S0301-0104(03)00025-9

in enhanced intervalence spectral features. In contrast, the overlap between the core orbitals and the Rydberg orbitals is poor because the Rydberg orbitals are located in the outer-wall. Hence, low spectral intensities are associated with Rydberg transitions.

Most of the prominent features attributable to shape resonance phenomena have been interpreted successfully within the independent particle model by applying dipole selection rules to identify which molecular orbitals may couple to specific shape resonantly enhanced channels. Such an analysis has enabled the major peaks occurring in the B 1s [1–6] photoabsorption spectra of BF_3, BCl_3 and BBr_3 (BI_3 has not been studied) to be assigned. For BF_3 and BCl_3 it is now fairly well established that the ground state valence shell electronic configuration, in D_{3h} symmetry, may be written as

$$(1a_1')^2(1e')^4(2a_1')^2(2e')^4(1a_2'')^2(3e')^4(1e'')^4(1a_2')^2 \quad \tilde{X}\,^1A_1'$$

where the numbering scheme is such that the core and inner-shell orbitals are ignored. The same configuration probably also applies to BBr_3 [9,10], but for BI_3 some details concerning the molecular orbital sequence remain uncertain [10]. This issue will be discussed in greater detail in Section 3.1.5. Ab initio calculations on BF_3 and BCl_3 indicate that the molecular orbitals of a_1', a_2'' and e' symmetry are responsible for B–X and for X–X bonding, where X = F or Cl, whilst those of a_2' and e'' symmetry are responsible for X–X bonding only [11]. The binding energies and characteristics of the unoccupied $2a_2''$, $3a_1'$, $4e'$, $3a_2''$ and $5e'$ orbitals have also been investigated [5,6,11–16].

The photoabsorption spectrum of BF_3, recorded in the vicinity of the boron K-shell edge [1–6], reveals two prominent features; an intense peak situated approximately 7 eV below the ionisation threshold and a broad maximum centred at ~2.2 eV in the continuum. Theoretical studies [5,6,12–14] have shown that these two features correspond to transitions into the $2a_2''$ orbital and into an e' shape resonance, respectively. In the photoabsorption spectra of BCl_3 and BBr_3, two strong peaks are observed below the B K-shell ionisation limit, but above threshold the spectra are structureless. Calculations predict that these two peaks should be associated with transitions into the $2a_2''$ and the $4e'$ orbitals [5]. In all three molecules, the B K-shell photoabsorption spectra reveal only very weak features that can be attributed to Rydberg transitions.

The valence shell photoabsorption spectra of the boron trihalides have received much less attention. Experiments have been carried out on BF_3 [17–19], BCl_3 [17,20–22], BBr_3 [17,20] and BI_3 [17], but only for BF_3 has a detailed interpretation been proposed for the absorption features observed above the ionisation threshold [18]. Parent and fragment photoion yield curves have been determined for BF_3 [23] and BCl_3 [24], but those for the parent ion do not seem to be in accord with the photoabsorption spectra. In view of the industrial relevance of the boron trihalides, particularly in regard to plasma etching, a more complete understanding of the valence shell photoexcitation and photoionisation processes is clearly desirable. In the present study, photoionisation yield curves of the boron trihalides have been measured from threshold to ~35 eV, and these have revealed many new features. Assignments have been proposed for some of the new structure and the importance of intervalence transitions is considered.

In addition to the yield curves, the valence shell threshold photoelectron spectra of the boron trihalides have been measured. These enable the energies of the vibrational modes in the ion to be determined. In some instances these spectra also provide information which helps characterise the excitation or ionisation processes. Valence shell photoelectron and threshold photoelectron spectra of the boron trihalides have been recorded previously using HeI [10,25–32], HeII [27,33] and continuum [34–38] sources. However, the majority of the work has concentrated on BF_3, and the threshold photoelectron spectra of BBr_3 and BI_3 have not been recorded.

Several theoretical studies [13,15,16,28,29, 39–41] have been performed which help interpret the valence shell photoelectron spectra of the boron trihalides. The most detailed calculations [40,41], carried out on BF_3, highlight the vibronic coupling effects prevalent in the valence shell ionic

states, and most of these predictions have now been verified experimentally [10,37,38,40]. The calculations reproduced successfully the complicated vibrational structure exhibited in the outer valence shell photoelectron bands of BF_3 and demonstrated that the two Jahn-Teller active modes show interference in all bands of E symmetry. The theoretical spectra illustrate the importance of both Jahn-Teller and pseudo-Jahn-Teller interactions. Unfortunately, calculations of a similar nature have not been performed on the other boron trihalides.

An additional effect that becomes progressively important in the heavier trihalides is the splitting, due to the large spin–orbit coupling, in the photoelectron bands associated with ionisation from degenerate orbitals. King et al. [29] and Dixon [42] have considered both first- and second-order spin–orbit coupling, and have demonstrated that these interactions strongly affect the photoelectron band structure in BBr_3 and BI_3. The recent HeI excited photoelectron spectra of the boron trihalides recorded by Shpinkova et al. [10] exhibit the predicted spin–orbit coupling effects quite clearly. However, their spectra revealed, particularly for BI_3, that the structure associated with the $3e'$ and $1e''$ orbitals is more complicated than would be expected due solely to spin–orbit effects, and that Jahn-Teller interactions might also be present.

Matrix isolation spectroscopy has been used to measure the infrared spectra of BF_3^+, BCl_3^+ and BBr_3^+, and provide vibrational energies [43–45]. Table 1 summarises the molecular ground state energies, characteristics and symmetries of the four normal modes of vibration in the boron trihalides [46].

2. Experimental apparatus and procedure

The experiments were carried out at the Daresbury Laboratory synchrotron radiation source using a threshold photoelectron and a photoion spectrometer system [47] attached to a 5 m normal incidence monochromator [48]. The experimental apparatus and procedure [47] have been described in detail previously so only a brief account will be given here.

The threshold photoelectron spectra and the total photoionisation yields could be recorded either separately or simultaneously. The advantage inherent to the simultaneous collection method lay in ensuring that the individual spectra were automatically energy calibrated against one another. In the spectrometer source region the monochromatic photon beam interacted with an effusive beam of the gas under investigation. A small electric field was used to extract the threshold (zero kinetic energy) photoelectrons and all the photoions. The electron detection system consisted of a lens optimised for high transmission of low energy electrons, followed by a hemispherical electrostatic analyser. The ions were propelled through a drift tube. Channeltrons were used to detect the electrons and ions. Lithium fluoride, indium or tin filters could be inserted into the photon beam to partially suppress higher order radiation. After passing through the interaction region the incident radiation impinged upon a sodium salicylate coated screen and the resulting fluorescence was detected with a photomultiplier. This signal could be used for normalisation purposes. All the samples were held at room temperature and entered the spectrometer through a heated inlet system.

Table 1
Summary of the molecular ground state energies, characteristics and symmetries of the four normal modes of vibration in the boron trihalides [46]

Normal mode	Vibrational energy (meV)			
	BF_3	BCl_3	BBr_3	BI_3
ν_1 (a_1') symmetric stretching	110.1	58.4	34.5	23.6
ν_2 (a_2'') out-of-plane bending	86.4	58.4	47.0	42.0
ν_3 (e') asymmetric stretching	181.4	122.3	102.5	88.0
ν_4 (e') asymmetric bending	59.6	30.1	18.6	12.4

Energy calibration was accomplished by recording spectra of a mixture of the sample and two inert gases.

3. Results and discussion

3.1. Valence shell threshold photoelectron spectra

3.1.1. Overview

The designation of the ionic states formed in the boron trihalides, particularly those in BBr_3 and BI_3, requires the use of extended point group notation to take into account the spin–orbit coupling in the orbitally degenerate states. In D_{3h} symmetry, spin–orbit effects split the degenerate electronic states as follows: $E' \rightarrow E_{3/2} + E_{5/2}$ and $E'' \rightarrow E_{1/2} + E_{3/2}$. The non-degenerate A_1' and A_2' states become $E_{1/2}$ components under the symmetry of the extended point group, and the A_1'' and A_2'' states become $E_{5/2}$ components [49]. Calculations performed by Dixon [42] demonstrate that spin–orbit coupling effects are significant for the $1e''$ and $3e'$ orbitals in BBr_3. If it is assumed that the spin–orbit coupling parameter is negative, then the first-order interaction splits the $^2E'$ state, with the $E_{5/2}$ component being lower in energy than the $E_{3/2}$ component. However, the first-order interaction will not split the $E_{1/2}$ and $E_{3/2}$ components of the $^2E''$ state because the $1e''$ molecular orbital is formed from a combination of out-of-plane bromine 4p orbitals, and therefore the projection of the orbital angular momentum on the threefold symmetry axis is zero [50]. The second-order spin–orbit interaction can couple components formed from different electronic states, with the strongest interaction separating the $E_{3/2}$ components of the $^2E'$ and $^2E''$ states. In addition to the splitting of degenerate states by spin–orbit coupling, the ^2E states can have their degeneracy lifted by Jahn-Teller interactions. In D_{3h} symmetry, the Jahn-Teller active vibrational modes have e' symmetry in both the $^2E'$ and $^2E''$ electronic states.

Fig. 1 shows threshold photoelectron spectra of the boron trihalides encompassing the entire valence shell region. A comparison between the HeI excited photoelectron spectra [10] and the threshold photoelectron spectra shows that those for BI_3 strongly resemble one another, but as the halogen atom becomes lighter the similarity decreases. This change in the spectra is particularly evident in the photoelectron bands associated with the three outermost orbitals. In BI_3, the threshold photoelectron spectrum (TPES) displays five distinct peaks due to ionisation from these three orbitals, and very similar features occur in the HeI excited spectrum [10]. However, this resemblance almost vanishes in BF_3, with a single prominent structured peak replacing the three features observed in the HeI excited spectrum.

The threshold photoelectron spectra suggest that the single particle model of ionisation [51] holds for the five outermost orbitals in all the boron trihalides. This is also the case for the $2a_1'$ orbital in BF_3 [52], and possibly in BCl_3. However, in BBr_3 and BI_3 the main-line associated with the $2a_1'$ orbital is embedded in a continuum due to configuration interaction states. For the $1a_1'$ and $1e'$ inner valence orbitals the single particle model of ionisation breaks down, and electron correlation leads to a redistribution of the intensity associated with the single-hole states amongst numerous satellites. For these two orbitals no main-lines can be distinguished. The spectra show that the contribution from the features involving the inner valence orbitals increases as the halogen atom becomes larger. In this respect the spectra for the boron trihalides are similar to those for the silicon tetrahalides [53].

A summary of the binding energies and assignments for the structure appearing in the threshold photoelectron spectra of the boron trihalides is provided in Table 2.

3.1.2. Boron trifluoride

The outer valence shell TPES of boron trifluoride is displayed in greater detail in Figs. 2–4. To a large extent the spectrum is similar to that reported recently by Yencha et al. [38] and as a consequence the present discussion concentrates on those aspects where the spectra, or the interpretation of the observed features, differ. In the binding energy range 15.6–17.0 eV, the stucture occurring in the TPES of BF_3 is very different to that appearing in the HeI excited photoelectron spectrum where two broad features, associated

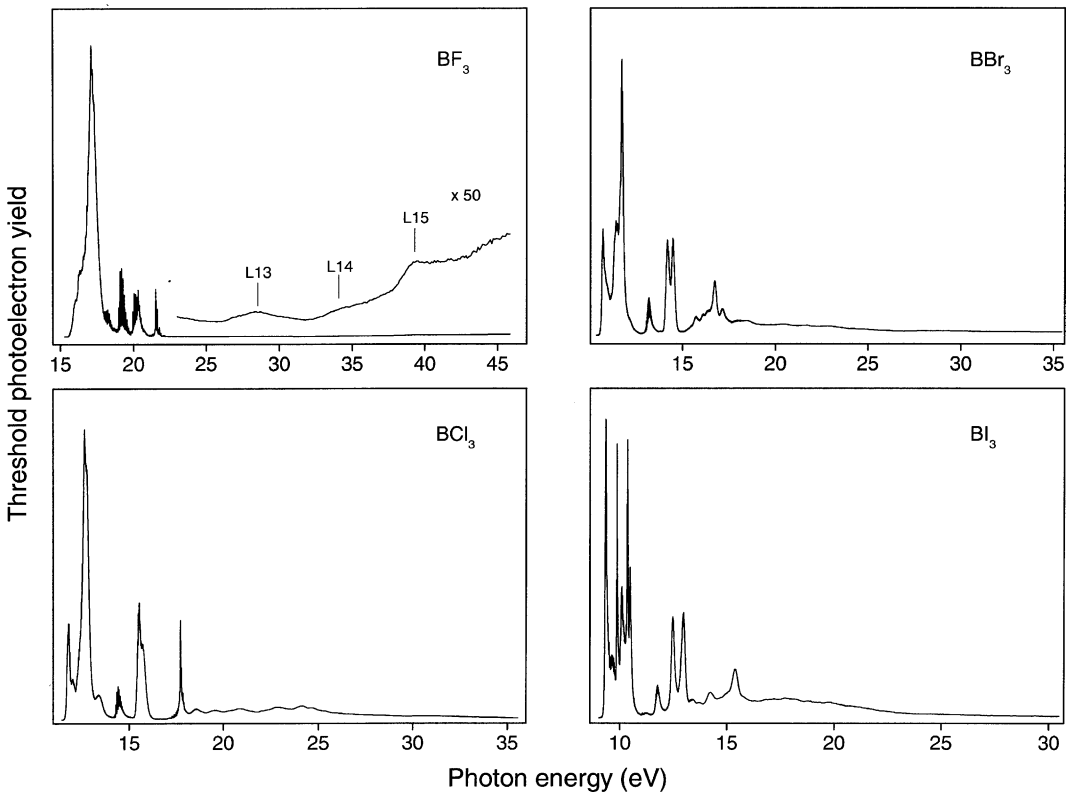

Fig. 1. The complete valence shell threshold photoelectron spectra of the boron trihalides.

with the $\tilde{X}^2A_2'$ and the $\tilde{A}^2E''$ states, are observed [10]. In this region the threshold photoelectron intensity exhibits a gradual rise and reaches a maximum at 17.123 eV, which correlates with the vertical ionisation energy of the $\tilde{B}^2E'$ state [10]. Superimposed upon this rise is a group of peaks, most of which can be attributed to autoionisation from Rydberg states belonging to an s-type series ($\delta \sim 1.0$) converging onto the $\tilde{B}^2E'$ state ionisation threshold. In addition to the features corresponding to the vibrationally unexcited series, three peaks, associated with the $n = 5$, 6 or 7 members of the vibrationally excited series with $v_1' = 1$, can be observed. Little support can be found for the $v_1' = 2$ series identified by Hagenow et al. [18] and by Yencha et al. [38]. Furthermore, there is no evidence, either in the present TPES or in that recorded by Batten et al. [34], of the two vibrational progressions, reported by Yencha et al, between 15.5 and 16.2 eV.

Between 17.9 and 18.95 eV the TPES (Fig. 2) exhibits features due to autoionisation from Rydberg states belonging to series converging onto the $\tilde{D}^2E'$ state ionisation threshold. Similar structure has been reported by Yencha et al. and assigned to overlapping and unresolved 3pσ and 3pπ Rydberg systems, in accordance with an earlier interpretation [18]. As will be shown in Section 3.2.2, the features due to autoionisation from Rydberg series converging onto the $\tilde{D}^2E'$ state ionisation threshold, or from states associated with intervalence transitions, appear more clearly in the photoion yield curves. Therefore discussion of this structure will be deferred.

Ionisation from the $1a_2''$ orbital results in a threshold photoelectron band (Fig. 3) displaying an extended progression involving the v_1^+ mode. An analysis of the spectrum yields a value of ~96 meV for this mode, in accordance with previous investigations.

Table 2
Summary of the binding energies and possible assignments of structure occurring in the threshold photoelectron spectra of the boron trihalides[a]

Boron trifluoride			Boron trichloride			Boron tribromide			Boron triiodide		
Probable orbital and transition		Energy (eV)	Probable orbital and transition		Energy (eV)	Probable orbital and transition		Energy (eV)	Probable orbital and transition		Energy (eV)
			$1a_2'$	L16	11.637	$1a_2'$	L52	10.656	$1a_2'$	L74	9.339
				L17	11.669		L53	10.690		L75	9.358
				L18	11.690		L54	10.717		L76	9.405
				L19	11.718						
				L20	11.741						
				L21	11.760						
				L22	11.785						
				L23	11.815						
				L24	11.833						
			$1e''$	L25	12.03	$1e''/3e'$	L55	11.344	$3e'/1e''$	L77	9.847
				L26	12.230		L56	11.395		L78	9.867
				L27	12.265		L57	11.447		L79	9.888
				L28	12.308		L58	11.485		L80	9.908
				L29	12.344		L59	11.506		L81	9.952
				L30	12.378		L60	11.615		L82	10.029
				L31	12.423		L61	11.674		L83	10.095
							L62	11.713		L84	10.161
$3e' \rightarrow ns$ ($\delta \sim 1.0$)			$3e'$	L32	12.506		L63	11.761		L85	10.196
	$n = 5$	16.265		L33	12.617		L64	12.17		L86	10.351
		16.340		L34	12.647					L87	10.470
	6	16.573		L35	12.671					L88	10.481
		16.660		L36	12.750					L89	10.524
	7	16.740		L37	12.784						
		16.838		L38	13.41						
	8	16.838									
	9	16.908									
	10	16.948									
	L1	16.040									
	L2	16.468									
	L3	17.023									
	L4	17.073									
$3e'$	L5	17.123									
	L6	17.199									
	L7	17.293									
	L8	17.410									
	L9	17.501									
$1a_2''$	0_0^0	18.983	$1a_2''$	0_0^0	14.191	$1a_2''$	0_0^0	12.938	$1a_2''$	0_0^0	11.582
	1_0^1	19.079		1_0^1	14.249		1_0^1	12.973		1_0^1	11.604

	1_0^2	19.175		1_0^2	14.308		1_0^2	13.008		1_0^2	11.627
	1_0^3	19.269		1_0^3	14.361		1_0^3	13.040		1_0^3	11.650
	1_0^4	19.367		1_0^4	14.414		1_0^4	13.074		1_0^4	11.673
	1_0^5	19.462		1_0^5	14.468		1_0^5	13.106		1_0^5	11.696
	1_0^6	19.557		1_0^6	14.520		1_0^6	13.138		1_0^6	11.717
	1_0^7	19.652		1_0^7	14.570		1_0^7	13.168		1_0^7	11.739
	1_0^8	19.752		1_0^8	14.619		1_0^8	13.200		1_0^8	11.761
				1_0^9	14.670		1_0^9	13.233		1_0^9	11.784
				1_0^{10}	14.720		1_0^{10}	13.263		1_0^{10}	11.805
							1_0^{11}	13.293		1_0^{11}	11.826
							1_0^{12}	13.324		1_0^{12}	11.846
							1_0^{13}	13.354		1_0^{13}	11.865
							1_0^{14}	13.383			
							1_0^{15}	13.414			
2e′	0_0^0	19.943	2e′	0_0^0	15.317	2e′ P1	1	14.086	2e′ P5	1	12.432
	2_0^0	19.977		2_0^0	15.344		2	14.116		2	12.453
	4_0^1	20.002		1_0^1	15.376		3	14.146		3	12.473
	1_0^1	20.036		$2_0^1 1_0^1$	15.393		4	14.175		4	12.491
	$2_0^1 1_0^1$	20.068		$4_0^1 1_0^1$	15.406		5	14.204			
	$4_0^1 1_0^1$	20.092		1_0^2	15.427		6	14.232	P6	1	12.828
	1_0^2	20.128		$2_0^1 1_0^2$	15.446		7	14.262		2	12.852
	$2_0^1 1_0^2$	10.160		$4_0^1 1_0^2$	15.457					3	12.875
	$4_0^1 1_0^2$	20.184		1_0^3	15.477	P2	1	14.103		4	12.897
	1_0^3	20.220		$2_0^1 1_0^3$	15.493		2	14.134		5	12.917
	$2_0^1 1_0^3$	20.247		$4_0^1 1_0^3$	15.505		3	14.163		6	12.941
	$4_0^1 1_0^3$	20.275		1_0^4	15.525		4	14.193		7	12.960
	1_0^4	20.314		$2_0^1 1_0^4$	15.539		5	14.222		8	12.977
	$2_0^1 1_0^4$	20.340		$4_0^1 1_0^4$	15.554		6	14.250		9	12.999
	$4_0^1 1_0^4$	20.365		1_0^5	15.574					10	13.018
	1_0^5	20.404		$4_0^1 1_0^5$	15.604	P3	1	14.124			
	$2_0^1 1_0^5$	20.427		1_0^6	15.625		2	14.155			
	$4_0^1 1_0^5$	20.458		1_0^7	15.675		3	14.182			
	1_0^6	20.494		1_0^8	15.720		4	14.212			
	$2_0^1 1_0^6$	20.520		1_0^9	15.765		5	14.242			
	1_0^7	20.584		1_0^{10}	15.810		6	14.269			
	1_0^8	20.675		1_0^{11}	15.857						
	1_0^9	20.765				P4	1	14.338			
							2	14.375			
	L10	20.258					3	14.408			
	L11	20.353					4	14.439			
	L12	20.442					5	14.469			
							6	14.495			
							7	14.526			
							8	14.555			

Table 2 (*continued*)

Boron trifluoride			Boron trichloride			Boron tribromide		Boron triiodide	
Probable orbital and transition		Energy (eV)	Probable orbital and transition		Energy (eV)	Probable orbital and transition	Energy (eV)	Probable orbital and transition	Energy (eV)
$2a'_1$	0^0_0	21.534	$2a'_1$	0^0_0	17.711				
	1^1_0	21.634		1^1_0	17.758				
	1^2_0	21.733		1^2_0	17.811				
	3^1_0	21.787		3^1_0	17.843				
	1^3_0	21.838		$3^1_0 1^1_0$	17.895				
	$3^1_0 1^1_0$	21.886		$3^1_0 1^2_0$	17.946				
	$3^1_0 1^2_0$	21.990							
	1^5_0	22.034							
	L13	28.5		L39	18.54	L65	15.72	L90	13.37
	L14	34.1		L40	19.54	L66	16.11	L91	13.68
	L15	39.3		L41	20.37	L67	16.34	L92	14.24
				L42	20.87	L68	16.738	L93	14.95
				L43	21.48	L69	17.15	L94	15.385
				L44	22.01	L70	18.45		
				L45	22.33	L71	20.40		
				L46	22.85	L72	21.58		
				L47	24.12	L73	22.83		
				L48	24.65				
				L49	25.40				
				L50	25.91				
				L51	30.82				

[a] L, line; P, vibrational progression.

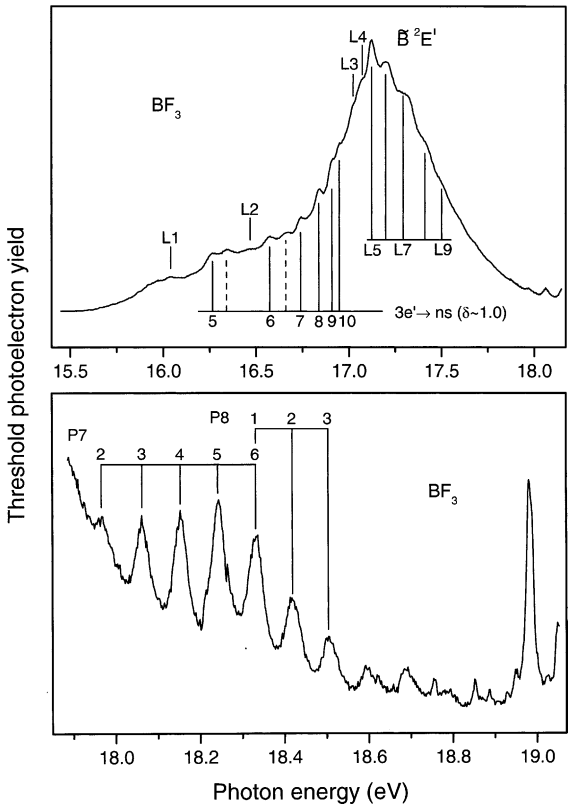

Fig. 2. TPES of BF_3, including the band associated with the $\tilde{B}^2E'$ state. Assignments and energy locations of the structure are given in Tables 2 and 3.

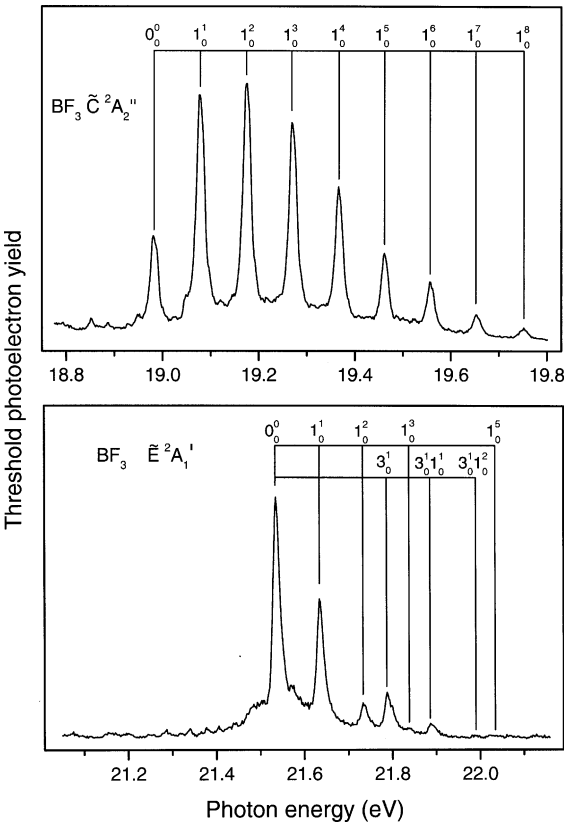

Fig. 3. TPES of BF_3 showing the bands associated with the $\tilde{C}^2A_2''$ and the $\tilde{E}^2A_1'$ states.

Three vibrational progressions, each involving excitation of the v_1^+ mode, are discernible in the threshold photoelectron band associated with the $\tilde{D}^2E'$ state (Fig. 4). In accordance with previous work, an energy of ~92 meV is obtained for the v_1^+ mode. We concur with Yencha et al. that the $v_1^+ = 0$ member of the strongest vibrational progression, at 19.943 eV, corresponds to the adiabatic ionisation energy. The second and third progressions are offset from the first by energy intervals of 32 and 56 meV, respectively, and in earlier studies [10,31,38] these intervals have been assigned to the v_2^+ and v_4^+ vibrational modes. However, a convincing explanation for the participation of the v_2^+ mode has yet to be given. The calculations performed by Haller et al. [41] to investigate the influence of two-mode Jahn-Teller interactions within the $\tilde{D}^2E'$ state suggest that the

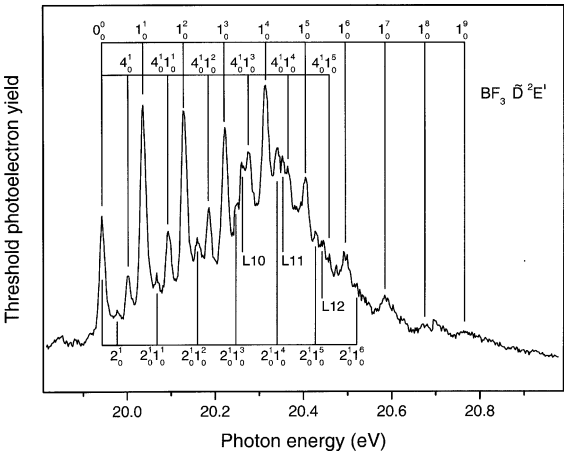

Fig. 4. TPES of BF_3 showing the band associated with the $\tilde{D}^2E'$ state.

vibrational structure in the associated photoelectron band should be due to excitation of the totally symmetric mode enhanced by excitation of both degenerate vibrations. Hagenow et al. [31] originally suggested that the occurrence of the v_2^+ mode might be due to coupling between the $\tilde{D}^2E'$ and the $\tilde{A}^2E''$ states, via this out-of-plane bending mode, even though the two states are separated by over 3 eV. The recent infrared spectra of BF_3 measured by Jacox and Thompson [44] give a value of 16.0 meV for the v_2^+ mode, which is half of the energy interval attributed to this mode in the photoelectron spectrum. Therefore the question arises as to whether the offset of 32 meV should be ascribed to a single or a double excitation of the v_2^+ mode.

Between 20.2 and 20.5 eV, the $\tilde{D}^2E'$ state threshold photoelectron band exhibits three peaks, labelled L10–L12, which do not belong to the three main vibrational progressions. In this energy region the ion yield curve of BF_3 (Section 3.2.2) displays structure due to Rydberg series converging onto the $\tilde{E}^2A_1'$ state limit. Therefore, it appears that these three additional peaks occurring within the $\tilde{D}^2E'$ state threshold photoelectron band may be attributed to autoionising Rydberg states.

The photoelectron band due to ionisation from the $2a_1'$ orbital occurs between 21.5 and 22.1 eV, and is shown in Fig. 3. Two vibrational progressions can be observed, each involving the v_1^+ mode, with one of the progressions having an additional excitation of the v_3^+ mode. An analysis of the spectrum yields values of 100 and 253 meV for the v_1^+ and v_3^+ modes, respectively, in good agreement with the recent results of Yencha et al. [38]. According to the calculations performed by Haller et al. [40], excitation of the v_3^+ mode occurs through a pseudo-Jahn-Teller interaction between the $\tilde{D}^2E'$ and the $\tilde{E}^2A_1'$ states. This prediction has been verified experimentally through vibrationally resolved measurements of the $\tilde{E}^2A_1'$ state photoelectron angular distributions [37].

The threshold photoelectron signal recorded in the inner valence region of BF_3 is substantially weaker than that measured in the corresponding regions of the heavier boron trihalides. The TPES (Fig. 1) shows a gradual rise in intensity as the energy increases, together with three superimposed broad features (L13–L15) at 28.5, 34.1 and 39.3 eV. The feature at 39.3 eV correlates with a doublet observed in the photoelectron spectrum of BF_3 recorded using a photon energy of 100 eV [37], and according to Green's function calculations [52] corresponds to processes associated with the $1a_1'$ and $1e'$ orbitals.

3.1.3. Boron trichloride

In the HeI excited photoelectron spectrum of BCl_3, ionisation from the outermost $1a_2'$ orbital results in a structureless peak, with a maximum at 11.72 eV and a 90 meV FWHM [10]. Although a corresponding prominent feature occurs in the TPES (Fig. 5), the leading edge displays complex but well developed vibrational structure and to higher energies a secondary peak is observed around 12.05 eV. The features (L16–L24) appearing between 11.6 and 11.85 eV have not been

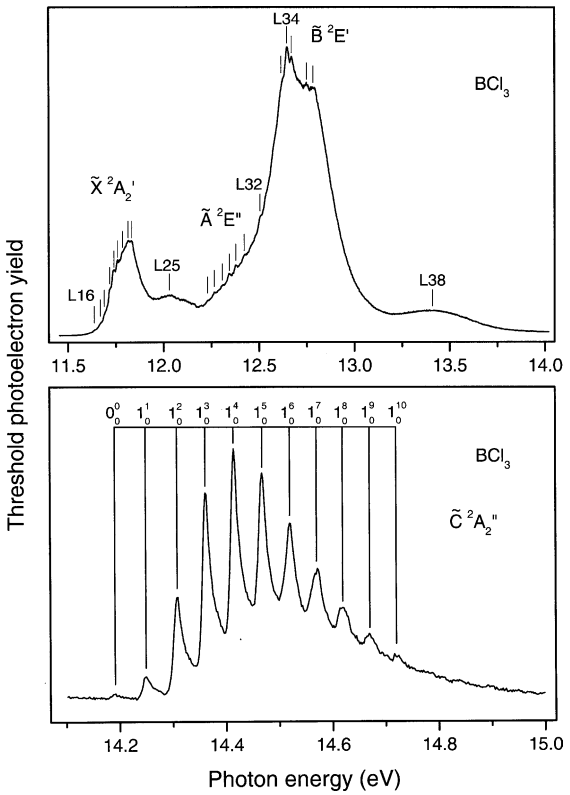

Fig. 5. TPES of BCl_3 showing the bands associated with the $\tilde{X}^2A_2'$, $\tilde{A}^2E''$, $\tilde{B}^2E'$ and $\tilde{C}^2A_2''$ states.

reported in the photoabsorption [21,22] or the fluorescence [21,22,54] spectra of BCl_3, and they do not occur in the ion yield curve (Section 3.2.3). This suggests that the structure might be due to vibrational excitations in the $\tilde{X}^2A_2'$ state. However, autoionisation from Rydberg or valence excited states also appears likely in this energy region. The separation between the peaks (~20–30 meV) is irregular and consequently it is unclear whether the structure should be attributed to one vibrational mode or two. As far as we are aware, the only mode in the ion for which a direct vibrational energy measurement has been made is ν_3^+. Infrared spectra give values of 135.1 meV [43] and 136.9 meV [45] for this mode. Our analysis of the vibrational structure in the BCl_3 $\tilde{D}^2E'$ state threshold photoelectron band leads to intervals of 19 and 30 meV, and these have been assigned to the ν_2^+ and ν_4^+ modes, respectively. Therefore we tentatively suggest that the features occurring between 11.6 and 11.8 eV involve excitation of the ν_4^+ mode, and possibly also the ν_2^+ mode.

One of the issues which requires clarification is whether the ground state of BCl_3^+ possesses D_{3h} symmetry or is distorted into a lower geometry. It is now established [41,55] that the ground state of BF_3^+ adopts a C_{2v} structure, arising from a pseudo-Jahn-Teller distortion, and Haller et al. [41] predict that the vibrational structure in the associated photoelectron band is dominated by the ν_3^+ and ν_4^+ modes. Theoretical work carried out by Baeck and Bartlett [16] suggests that the ground state of BCl_3^+ also adopts C_{2v} symmetry. However, they caution that more refined calculations might restore the structure to D_{3h} symmetry. Further theoretical investigations are needed to resolve this matter.

The peak at 11.833 eV in the TPES correlates with a feature in the ion yield curve (Section 3.2.3) attributed to the $3e' \rightarrow 5s$ transition, and the next member of this Rydberg series corresponds with the broad feature (L25) around 12.03 eV. A group of peaks, labelled L26–L31, occur in the TPES between 12.2 and 12.6 eV, and it is conceivable that these peaks constitute a vibrational progression with a spacing of ~39 meV. This structure coincides with a broad peak in the photoion spectrum ascribed to the $3e' \rightarrow 7s$ transition. However, in the HeI excited spectrum of BCl_3 [10] the $\tilde{A}^2E''$ state photoelectron band exhibits an extended vibrational progression, with a similar spacing, in the same binding energy region. Thus, it is uncertain whether the features discernible in the TPES should be attributed to autoionisation from vibrational levels in the Rydberg state, or to direct ionisation into the $\tilde{A}^2E''$ state. On balance, the latter explanation appears more likely. The peak separation suggests that the structure involves excitation of the ν_4^+ mode, but it is noticeable that the average spacing is greater than the 30 meV which we consider to be the vibrational energy of the ν_4^+ mode. Thus, the structure may not be due solely to a single vibrational mode.

The prominent doublet occurring between 12.5 and 13.0 eV in the TPES corresponds to the $E_{5/2}$ and $E_{3/2}$ spin–orbit split components of the $\tilde{B}^2E'$ state. It appears that resonant autoionisation is affecting the production process because in the TPES the two components are of almost equal strength whilst in the HeI excited spectrum the $E_{5/2}$ component is significantly more intense than the $E_{3/2}$ component. Several weak features are discernible in the peaks of the doublet and the energy intervals suggest that excitation of ν_4^+ may be responsible for this structure. The very broad peak (L38) with a maximum at 13.41 eV may be due to the $2e' \rightarrow 3p$ Rydberg transition and/or an intervalence transition. This issue is discussed in Section 3.2.3.

Analysis of the $\tilde{C}^2A_2''$ state threshold photoelectron band (Fig. 5), due to ionisation from the $1a_2''$ orbital, is straightforward, and gives an average separation of 53 meV for the ν_1^+ mode, in agreement with previous work. It is evident that the adiabatic energy is 14.191 eV, and that the lowest vibrational member has not been observed previously. In the TPES significant intensity appears between the main vibrational members, much greater than that observed in the HeI excited spectrum [10], due to autoionisation from Rydberg series converging onto vibrationally excited levels of the ion.

Ionisation from the $2e'$ orbital leads to a complicated threshold photoelectron band occurring in the binding energy range 15.3–16.0 eV (Fig. 6). The overall profile is similar to that observed in the HeI excited spectrum [10] but the two components

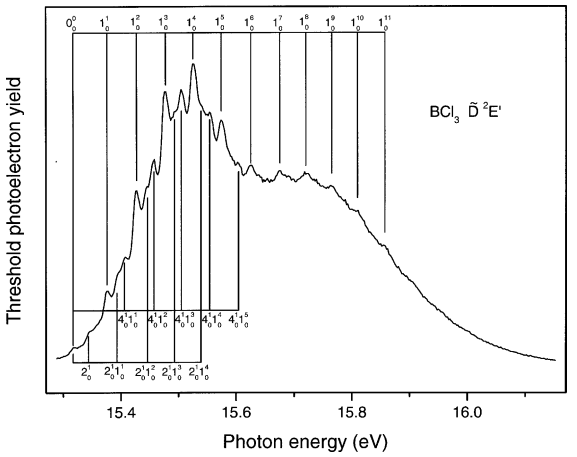

Fig. 6. TPES of BCl_3 showing the band associated with the $\tilde{D}^2E'$ state.

resulting from the spin–orbit coupling can be distinguished more clearly. Shpinkova et al. [10] suggested that the vibrational structure observed near the beginning of the band in the HeI excited spectrum should be interpreted in terms of two progressions, each involving excitation of the v_1^+ mode, with the second progression being offset from the first by ~30 meV. The TPES demonstrates that there are three progressions, each of which involves the v_1^+ mode, with the second and third progressions being offset from the first by 19 and 30 meV, respectively. Thus the vibrational structure in the $\tilde{D}^2E'$ state photoelectron band of BCl_3^+ is similar to that in the corresponding state of BF_3^+. As will be shown, this is also the case for BBr_3^+. We tentatively interpret the offsets as being due to single excitation of the v_2^+ and the v_4^+ modes. As in BF_3, the strongest vibrational progression in BCl_3 can be observed over both spin–orbit split components.

The vibrational structure in the $\tilde{E}^2A_1'$ state threshold photoelectron band of BCl_3 (Fig. 7) can be assigned in a manner similar to that used in the corresponding band of BF_3 (Fig. 3). Two progressions can be observed, each involving excitation of the v_1^+ mode, with one of the progressions having an additional excitation of the v_3^+ mode. The present spectrum yields a value of 132 meV for the v_3^+ mode, in good agreement with previous results [43,45]. Numerous peaks occur in the

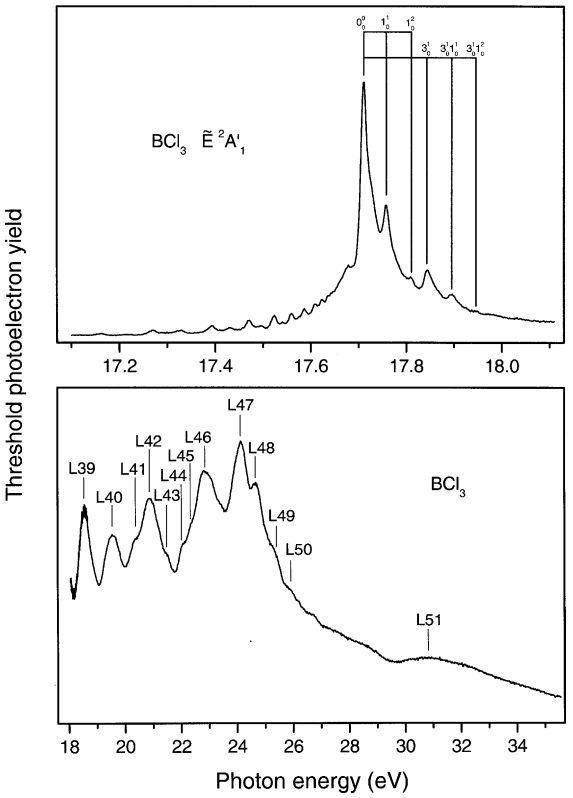

Fig. 7. TPES of BCl_3 showing the band associated with the $\tilde{E}^2A_1'$ state and the structure due to the inner valence orbitals.

binding energy range 16.6–17.7 eV due to autoionisation from Rydberg states belonging to p- and d-type series converging onto the $\tilde{E}^2A_1'$ state ionisation threshold. Structure due to these series appears prominently in the ion yield curves, so discussion will be deferred.

In comparison with BF_3, the features involving the $1a_1'$ and $1e'$ inner valence orbitals in BCl_3 are more prominent and have shifted to lower binding energies. This shift may be related to the lower binding energy of 24.54 eV for the Cl 3s subshell, compared to that of 37.85 eV for the F 2s subshell. The inner valence TPES of BCl_3, shown in Fig. 7, is somewhat similar to that of $SiCl_4$ [53].

3.1.4. Boron tribromide

Ionisation from the three outermost orbitals in BBr_3 results in photoelectron bands occurring in the binding energy range 10.5–12.5 eV. It is

noticeable that the features, associated with these orbitals, in the TPES (Fig. 8) resemble to a certain extent the corresponding features in the HeI excited spectrum [10]. The $\tilde{X}^2A_2'$ state threshold photoelectron band exhibits a maximum at 10.690 eV and some weak structure is discernible in the peak. The energy intervals suggest that these features could be due to the ν_1^+ mode.

The interpretation of the TPES of BBr_3 in the binding energy range 11.2–12.0 eV is less straightforward and would be difficult to accomplish without recourse to the HeI excited spectrum [10]. In the latter spectrum, ionisation from the $1e''$ and the $3e'$ orbitals resulted in complicated structure occurring in the binding energy range 11.1–11.9 eV. Five peaks were discernible with maxima at 11.319, 11.389, 11.489, 11.618 and 11.722 eV. Using the calculated energy levels [42], and the experimental energy separations, Shpinkova et al.

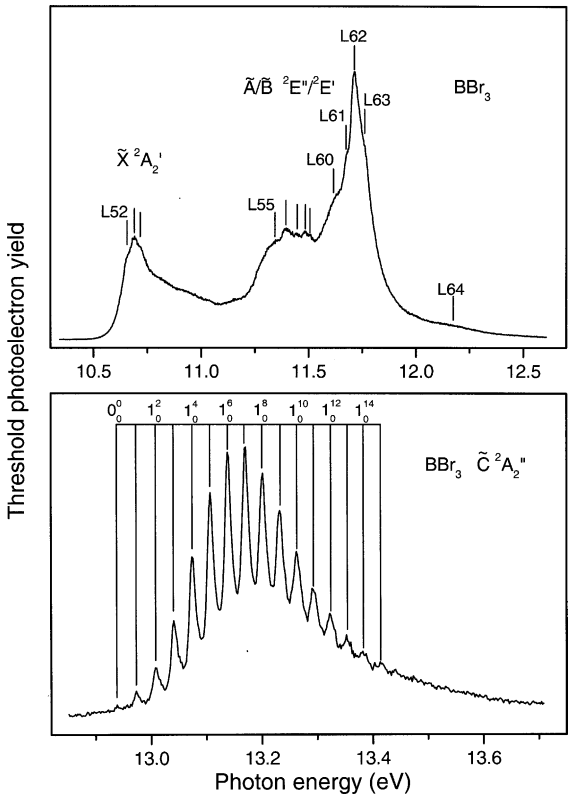

Fig. 8. TPES of BBr_3 showing the bands associated with the $\tilde{X}^2A_2'$, $\tilde{A}/\tilde{B}^2E''/^2E'$ and $\tilde{C}^2A_2''$ states.

[10] speculated that the two pairs of peaks at 11.389 and 11.618 eV, and at 11.489 and 11.722 eV correspond to the spin–orbit split components arising from the $1e''$ and $3e'$ orbitals. The prominent peak at 11.722 eV was assigned to the $E_{3/2}$ component of the $\tilde{B}^2E'$ state, and Jahn-Teller interactions were invoked to account for the extra structure.

Based upon these assignments it appears reasonable to associate the intense peak occurring at 11.713 eV in the TPES with the $E_{3/2}$ component of $\tilde{B}^2E'$ state. This peak has additional structure on both the high and the low binding energy shoulders, and one of these features (L60), at 11.615 eV, correlates with a prominent peak occurring in the HeI excited spectrum. Unfortunately the assignment of this peak has yet to be firmly established. The very broad feature centred around 11.4 eV in the TPES displays several weak peaks (L55–L59) between 11.3 and 11.5 eV. Two of the peaks correspond with features tentatively ascribed to the lower energy spin–orbit components of the $\tilde{A}^2E''$ and the $\tilde{B}^2E'$ states in the HeI excited spectrum [10]. Alternatively, these two features could correspond to the $E_{1/2}$ and $E_{3/2}$ components of the $\tilde{A}^2E'$ state.

As with the corresponding bands in BF_3 and BCl_3, the assignment of the vibrational structure observed in the BBr_3^+ $\tilde{C}^2A_2''$ state is unambiguous. The band, shown in Fig. 8, exhibits a progression in the ν_1^+ mode, with an average spacing of 32 meV.

Spin-orbit interactions lead to the threshold photoelectron band (Fig. 9) associated with the $2e'$ orbital forming a distinct doublet. The vibrational structure in the $E_{5/2}$ component can be assigned to three progressions (P1–P3), each involving excitation of the ν_1^+ mode. The second and third progressions are offset from the first by intervals of 8 and 18 meV, and these energies are attributed to the ν_2^+ and the ν_4^+ modes, respectively. The vibrational peaks in the higher binding energy, $E_{3/2}$ component, are broad and almost certainly members from more than one progression are contributing to each observed peak. An energy of ~30 meV is obtained for the ν_1^+ mode from an analysis of the $\tilde{D}^2E'$ state vibrational structure.

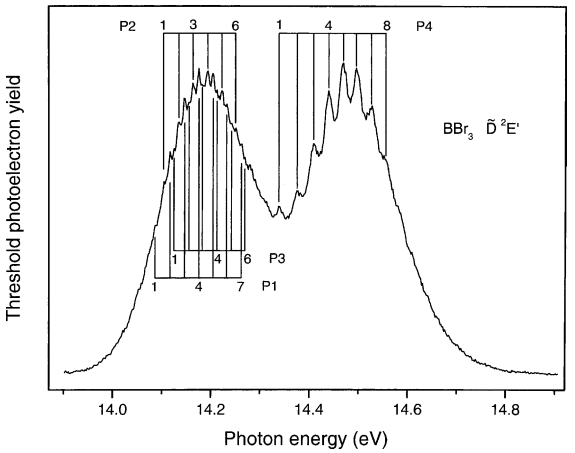

Fig. 9. TPES of BBr_3 showing the band associated with the $\tilde{D}^2E'$ state.

Features due to the $1a_1'$, $1e'$ and $2a_1'$ orbitals occur in the binding energy range 15–36 eV and are shown in Fig. 10. The most prominent peak (L68), at 16.738 eV, correlates with the main-line ascribed to the $2a_1'$ orbital in the HeI excited spectrum [10]. Interestingly, that spectrum exhibited another feature at 17.16 eV, and Shpinkova et al. [10] suggested that it might be associated with a satellite state resulting from configuration interaction. It is now evident that the single particle model of ionisation breaks down for the $1a_1'$ and

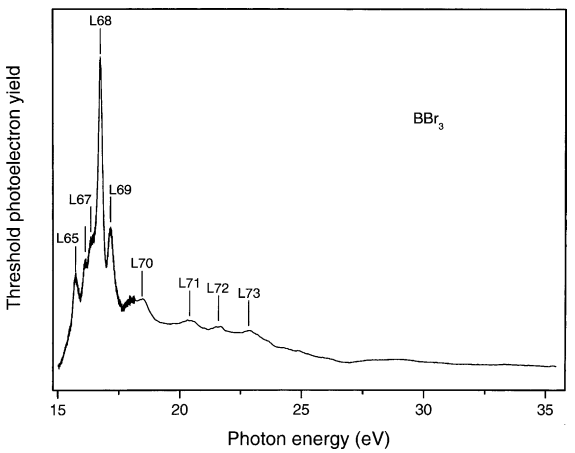

Fig. 10. TPES of BBr_3 showing the feature (L68) associated with the $2a_1'$ orbital and the structure due to the inner valence orbitals.

$1e'$ orbitals, and also to some extent for the $2a_1'$ orbital, and that electron correlation leads to numerous satellite states throughout the 15–36 eV region.

3.1.5. Boron triiodide

The assignment of the photoelectron bands due to ionisation from the $3e'$ and $1e''$ orbitals in BI_3 is uncertain because it is not known whether the electronic configuration is $1a_2'$, $3e'$, $1e''$ or $1a_2'$, $1e''$, $3e'$, in order of increasing binding energy. This issue has been the subject of much debate [10,27–29]. The energy level spacings predicted by King et al. [29] and Dixon [42] indicate that if the $3e'$ orbital is more tightly bound than the $1e''$ orbital, then spin–orbit interactions result in three of the components being clustered together at a low binding energy, whilst the fourth component lies at a significantly higher energy. On the other hand, if the $1e''$ orbital is more tightly bound than the $3e'$ orbital, spin–orbit interactions lead to the four components being more or less equally spaced in energy. As a result of a comparison between these predictions and the experimental spectrum for BI_3, Shpinkova et al. [10] marginally favoured the configuration for this molecule being $1a_2'$, $3e'$, $1e''$. Although the photoion yield curves for BI_3 (Section 3.2.5) display two Rydberg series converging onto the ionisation threshold at 9.865 eV, and one onto the limit at 10.351 eV, the selection rules are such that these cannot be used to distinguish between the alternative molecular orbital sequences. Therefore, the configuration of $1a_2'$, $3e'$, $1e''$ is used in the present work.

The asymmetric threshold photoelectron peak with a maximum at 9.339 eV (Fig. 11) correlates with a feature attributed to the $\tilde{X}^2A_2'$ state in the HeI excited spectrum. A shoulder at 9.358 eV (L75) may be associated with excitation of the ν_1^+ mode. In the binding energy range ~9.5–9.8 eV, the TPES displays many low intensity peaks, and most of these can be assigned to two Rydberg series converging onto the limit at 9.865 eV associated with the $E_{5/2}$ component of the $\tilde{A}^2E'$ state. These series will be discussed in Section 3.2.5 because they can be observed more clearly in the photoion yield curve than in the TPES.

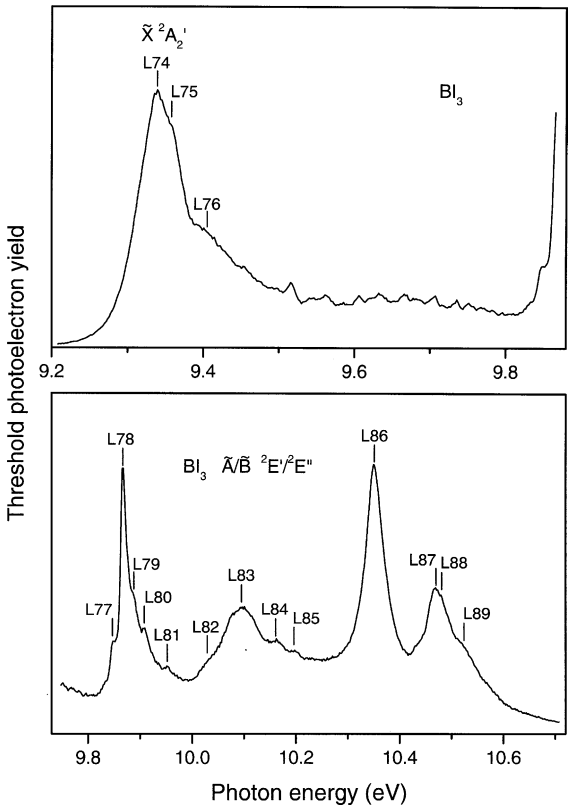

Fig. 11. TPES of BI_3 showing the bands associated with the $\tilde{X}^2A_2'$ and the $\tilde{A}/\tilde{B}^2E'/^2E''$ states.

Four prominent peaks (L78, L83, L86 and L87) appear in the TPES between 9.8 and 10.7 eV (Fig. 11), and these correlate with the four components which result from the first- and second-order spin–orbit interactions involving the 3e′ and 1e″ orbitals [29,42]. The peaks at 9.865 and 10.351 eV are noticeably sharper than those at 10.095 and 10.470 eV. Shpinkova et al. have speculated that Jahn-Teller interactions may contribute to the widths of the second pair of peaks. The peak with a maximum at 9.865 eV exhibits structure on both the leading and falling edges. That on the high binding energy side could be interpreted as a vibrational progression involving the ν_1^+ mode, with an energy of about 22 meV. If this is the case, then L79 and L80 correspond to the 1_0^1 and the 1_0^2 transitions, respectively, and the peak at 9.952 eV may be associated with either the 1_0^4 transition or possibly to the excitation of some other mode. The shoulder at 9.847 eV probably represents a hot band transition.

In common with the three lighter boron trihalides, the BI_3^+ $\tilde{C}^2A_2''$ state threshold photoelectron band, shown in Fig. 12, exhibits a vibrational progression due to excitation of the ν_1^+ mode. The average vibrational spacing is 22 meV, in agreement with previous work [10].

Vibrational structure can be observed on both spin–orbit split components of the $\tilde{D}^2E'$ state threshold photoelectron band shown in Fig. 13. The average separation between the peaks is ~21 meV, which suggests that the ν_1^+ mode is being excited. However, many of the peaks, and particularly those discernible in the higher energy $E_{3/2}$ component, display a complex profile. Superior resolution would probably reveal three progres-

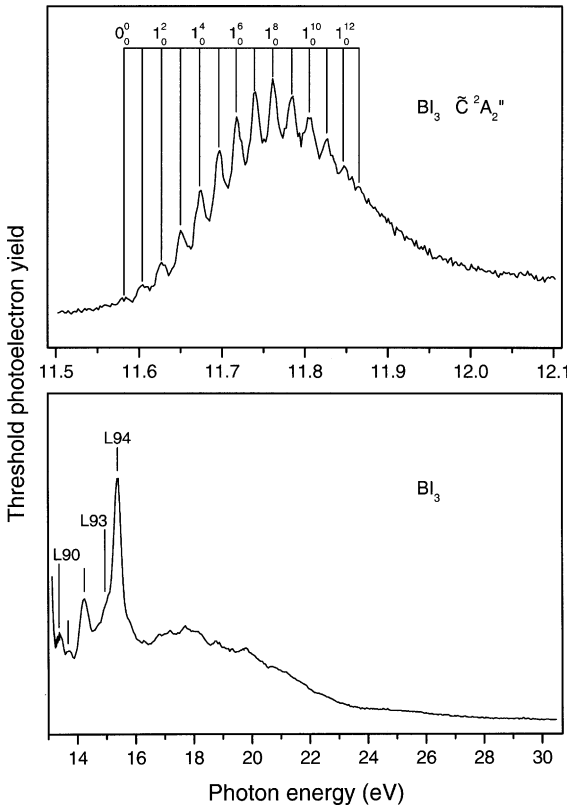

Fig. 12. TPES of BI_3 showing the band associated with the $\tilde{C}^2A_2''$ state. L94 is due to the $2a_1'$ orbital and the remaining features involve the inner valence orbitals.

sions, as observed in the $\tilde{D}^2E'$ state photoelectron bands of the lighter boron trihalides.

The TPES encompassing the inner valence region is shown in Fig. 12. The prominent peak (L94) at 15.385 eV can be identified with the main-line due to ionisation from the $2a_1'$ orbital, and three further features occur at 13.37, 13.68 and 14.24 eV. In BI_3, the continuum formed by the photoelectron bands associated with configuration interaction states extends from ~12 to 30 eV, and Fig. 1 illustrates that this contribution constitutes a significant part of the total intensity.

3.2. Photoionisation yield curves

3.2.1. Overview

The valence shell total photoionisation yield curves of the boron trihalides are shown in Fig. 14 and a summary of the assignments proposed for the observed structure is given in Table 3. The present curves are not in accord with the parent ion yields reported for BF_3 [23] or BCl_3 [24], but they exhibit reasonable agreement with the photoabsorption spectra of these two molecules [18,19,22]. To the best of our knowledge, measurements of the photoabsorption spectra of BBr_3 [17,20] and BI_3 [17] have been limited to energies below the ionisation threshold. The present photoion yield curves encompass a wider photon energy range and/or have been recorded with superior resolution than employed in earlier work and these improvements have enabled new Rydberg series to be observed in all four molecules. In some cases, particularly for BF_3, we have been able to identify vibrational progressions associated with a specific Rydberg state, but have been unable to assign the Rydberg state itself. Two difficulties contribute towards this unsatisfactory situation. The first is that some of the vibrational progressions heavily overlap one another and the second is that regular Rydberg series, containing states associated with sequential values of the principal quantum number (n), are often not observed. In several instances, if the Rydberg formula is used to designate the state associated with a particular vibrational progression then a rather large value of n is obtained, and the lower members of the series cannot necessarily be observed in the ion yield curves. We conclude that intervalence transitions, or transitions to upper levels of mixed Rydberg/valence character are responsible for some of the structure and may be perturbing the normal Rydberg series.

As previous work [1–6,12–14] has established that the B 1s photoabsorption spectra of BF_3, BCl_3 and BBr_3 are dominated by features attributable to transitions into virtual orbitals, and that structure due to Rydberg transitions is weak, it appears not unreasonable to expect that intervalence transitions play a major role in the valence shell excitations. A similar situation exists for SF_6, which is perhaps the best known example of a molecule exhibiting shape resonantly enhanced transitions both below and above the core and inner-shell ionisation thresholds [56–60]. The valence shell photoabsorption spectrum of SF_6 [61] mirrors this behaviour with only a few very weak vibrational progressions being attributable to Rydberg states. In contrast, many strong features due to intervalence transitions are discernible. It appears that the valence shell spectra of the boron trihalides follow this pattern.

Our assignments for the features occurring in the ion yield curves rely heavily on an assessment of term values, and also on the reasonable assumption that a broadly similar interpretation should be applicable to all four boron trihalides. In regard to this second criterion, it needs to be borne in mind that the B 1s photoabsorption spectra of these molecules show that transitions into the $4e'$ orbital occur above the ionisation limit for BF_3, whereas for BCl_3 and BBr_3 (and we assume also for BI_3) they appear below threshold. Dipole selection rules forbid transitions into the $3a_1'$ orbital from the B 1s shell (of a_1' symmetry) of the boron trihalides. The term values for transitions into the $2a_2''$ and $4e'$ orbitals from the B 1s shell are given in Table 4. However, the energy locations of such transitions tend to move a few eV towards higher energy for valence shell excitation. This shift has already been confirmed for transitions into the $4e'$ orbital of BF_3 through a comparison of the calculated [13] and experimentally observed [35,37] locations. The comparison also showed that the predicted shape resonantly enhanced features were not observed in all channels.

Table 3
Summary of the energies and possible assignments of structure occurring in the photoionisation yield curves of the boron trihalides[a]

Boron trifluoride			Boron trichloride			Boron tribromide			Boron triiodide		
Probable orbital and transition		Energy (eV)	Probable orbital and transition		Energy (eV)	Probable orbital and transition		Energy (eV)	Probable orbital and transition		Energy (eV)
	L95	15.943	$3e' \rightarrow ns(a_1')$			$3e' \rightarrow ns(a_1')$			$3e'(?) \rightarrow ns(a_1')$		
	L96	16.337	$\delta \sim 1.1$			$\delta \sim 1.0$			$\delta \sim 0.7$–0.8		
	L97	16.472		$n = 5$	11.832		$n = 5$	10.901		$n = 7$	9.517
	L98	16.565		6	12.058		6	11.172		8	9.608
	L99	16.657		7	12.240		7	11.312		9	9.668
	L100	16.737		8	12.385					10	9.706
	L101	16.832				$3e' \rightarrow np$				11	9.736
	L102	16.903		L105	12.863	$\delta \sim 0.5$				12	9.757
	L103	16.941					$n = 6$	11.273		13	9.774
	L104	17.575	P17	1	13.400		7	11.391		14	9.787
				2	13.448		8	11.469		15	9.798
P7	1	17.895		3	13.510		9	11.516		16	9.807
	2	17.985		4	13.573					17	9.815
	3	18.075		5	13.630	L106		11.99		18	9.822
	4	18.166		6	13.681	L107		12.22			
	5	18.255		7	13.730				$3e'(?) \rightarrow np$		
	6	18.343		8	13.777	P23	1	12.639	$\delta \sim 0.3$		
							2	12.668		$n = 6$	9.444
P8	1	18.330	P18	1	13.819		3	12.701		7	9.567
	2	18.424		2	13.865		4	12.731		8	9.639
	3	18.516		3	13.918		5	12.762		9	9.683
	4	18.608		4	13.974		6	12.797		10	9.718
				5	14.026		7	12.828		11	9.748
P9	1	18.343		6	14.079		8	12.860			
	2	18.438		7	14.130		9	12.891	$1e''(?) \rightarrow np$		
	3	18.539		8	14.178		10	12.923	$\delta \sim 0.3$		
	4	18.635		9	14.231					$n = 4$	9.365
	5	18.733		10	14.286	P24	1	12.789		5	9.705
				11	14.337		2	12.816		6	9.922
P10	1	18.609		12	14.392		3	12.848		7	10.049
	2	18.707					4	12.880		8	10.124
	3	18.805	P19	1	13.838		5	12.911		9	10.175
	4	18.903		2	13.897					10	10.205
	5	18.999		3	13.952	P25	1	12.957			
	6	19.094		4	14.008		2	12.992	L114		9.411
	7	19.189		5	14.062		3	13.023	L115		9.457
	8	19.285		6	14.117		4	13.053	L116		9.481
	9	19.381		7	14.165		5	13.084	L117		9.496
	10	19.477		8	14.213		6	13.116	L118		9.546

Table 3 (*continued*)

Boron trifluoride			Boron trichloride			Boron tribromide			Boron triiodide		
Probable orbital and transition		Energy (eV)	Probable orbital and transition		Energy (eV)	Probable orbital and transition		Energy (eV)	Probable orbital and transition		Energy (eV)
				9	14.267		7	13.146	L119		9.589
P11	1	18.673		10	14.313				L120		10.26
	2	18.772		11	14.371	P26	1	13.445	L121		10.30
	3	18.869					2	13.478	L122		10.38
	4	18.965	P20	1	14.891		3	13.506	L123		10.57
	5	19.062		2	14.943		4	13.538	L124		10.78
	6	19.159		3	14.999		5	13.567			
	7	19.256		4	15.049				P32	1	11.228
				5	15.101	P27	1	13.555		2	11.249
P12	1	18.826		6	15.149		2	13.584		3	11.265
	2	18.922		7	15.196		3	13.617		4	11.288
	3	19.019		8	15.253		4	13.650		5	11.310
	4	19.114		9	15.299					6	11.334
				10	15.351	P28	1	13.607		7	11.354
P13	1	18.944		11	15.400		2	13.637		8	11.377
	2	19.044		12	15.450		3	13.665		9	11.398
	3	19.144		13	15.498		4	13.700		10	11.421
	4	19.244					5	13.731		11	11.443
	5	19.337	P21	1	14.919		6	13.763		12	11.465
	6	19.428		2	14.970		7	13.794		13	11.487
	7	19.521		3	15.019					14	11.509
	8	19.619		4	15.068	P29	1	13.919		15	11.533
				5	15.119		2	13.949		16	11.556
P14	1	19.472		6	15.171		3	13.978		17	11.578
	2	19.573		7	15.222		4	14.008		18	11.600
	3	19.667		8	15.281		5	14.038		19	11.621
	4	19.759		9	15.334		6	14.068		20	11.642
	5	19.853		10	15.384		7	14.098		21	11.664
				11	15.433		8	14.128		22	11.687
P15	1	19.541		12	15.476		9	14.158		23	11.711
	2	19.636		13	15.517		10	14.187			
	3	19.733					11	14.215	P33	1	11.964
	4	19.828	P22	1	14.988		12	14.245		2	11.989
	5	19.922		2	15.038		13	14.275		3	12.009
				3	15.089		14	14.310		4	12.031
P16	1	19.879		4	15.139					5	12.054
	2	19.963		5	15.191	P30	1	13.929		6	12.079
	3	20.055		6	15.243		2	13.960		7	12.103
	4	20.146					3	13.989		8	12.124
	5	20.236	$2a_1' \rightarrow np(a_2'')$				4	14.018			

			$\delta \sim 0.5$				5	14.049	P34	1	12.201
$2a_1' \rightarrow nd$				$n = 3$	15.517		6	14.078		2	12.223
$\delta \sim -0.15$				4	16.623		7	14.106		3	12.245
	$n = 3$	20.170		5	17.041		8	14.134		4	12.268
	4	20.744		6	17.259		9	14.163		5	12.291
	5	21.031		7	17.385		10	14.193		6	12.309
				8	17.461		11	14.220		7	12.328
$2a_1' \rightarrow np(a_2'')$				9	17.514		12	14.250		8	12.349
$\delta \sim 0.5$				10	17.553		13	14.283		9	12.370
	$n = 4$	20.367		11	17.574		14	14.315		10	12.392
		20.462		12	17.598		15	14.342			
	5	20.850							P35	1	12.433
		20.947	$2a_1' \rightarrow np(e')$			P31	1	13.936		2	12.454
	6	21.084	$\delta \sim 0.4$				2	13.967		3	12.473
	7	21.196		$n = 3$	15.705		3	13.996		4	12.496
				4	16.670		4	14.025			
$2a_1' \rightarrow np(e')$					16.712		5	14.056	P36	1	12.601
$\delta \sim 0.4$				5	17.071		6	14.087		2	12.621
	$n = 7$	21.223			17.121		7	14.116		3	12.641
	8	21.300		6	17.277		8	14.146		4	12.665
					17.327					5	12.687
				7	17.399					6	12.709
					17.449					7	12.730
				8	17.475					8	12.754
				9	17.528					9	12.777
				10	17.563					10	12.797
				11	17.588					11	12.818
				12	17.611					12	12.840
										13	12.863
			$2a_1' \rightarrow nd$							14	12.882
			$\delta \sim 0.0$								
				$n = 4$	16.861					L125	13.07
					16.917					L126	13.59
				5	17.168					L127	14.24
				6	17.314					L128	14.70
				7	17.434					L129	16.94

[a] L, line; P, vibrational progression.

Table 4
Summary of the term values (eV) for B 1s level excitation in the boron trihalides [5]

Final orbital	Term value		
	BF_3	BCl_3	BBr_3
2p (a_2'')	7.3	7.4	7.0
3s + 3a_1'	4.6	3.7	4.1
3p (a_2'')	2.5	2.2	2.0
3p (e′)			
4p (a_2'')	1.1	1.1	1.3
4p (e′)		0.8	0.6
2p (e′)	−2.3	2.9	3.2

Planckaert et al. [20] have measured the photoabsorption spectra of BCl_3 and BBr_3 from threshold to ~10.5 eV, and these allow term values for valence shell excitations into the 2a_2'' and 3a_1' orbitals to be derived. The photoabsorption spectrum of BCl_3 has also been recorded by Lee et al. [22], with similar results. Maria et al. [17] have reported the photoabsorption spectra of all four boron trihalides at low photon energies. However their spectra do not agree with later work and have not been used to deduce term values. Our ion yield curve for BCl_3 displays structure due to p(a_2''), p(e′) and d-type Rydberg series, following excitation from the 2a_1' orbital. These three series have been used to derive term values for excitation into Rydberg orbitals. A summary of the valence shell term values is presented in Table 5. For the boron trihalides, the low-lying virtual valence orbitals have a_2'', a_1' and e′ symmetries, and selection rules allow the following transitions. Excitation into an a_2'' orbital may occur from orbitals of a_1' or e″ symmetry, and into an a_1' orbital from orbitals of a_2'' or e′ symmetry. Excitation into an e′ orbital is allowed from all orbitals except those of a_2'' symmetry.

The photoionisation yield curves exhibit vibrational progressions at the following energy intervals below the appropriate $\tilde{D}^2E'$ state ionisation threshold: BF_3, 1.9 eV; BCl_3, 0.3, 1.35 and 1.95 eV; BBr_3, 0.31, 0.76 and 1.66 eV; BI_3, 0.15, 0.65 and 1.45 eV. The principal difficulty encountered in assigning the valence shell absorption structure concerns the designation of the excited states associated with the vibrational progressions observed only a few tenths of an eV below the $\tilde{D}^2E'$ state limit. As Table 5 indicates, the term values of the intervalence transitions considered so far are too large to account for this structure.

A possible solution can be found in the theoretical study performed by Baeck and Bartlett [16] where valence shell transition energies were

Table 5
Summary of the term values (eV) for valence shell excitation in BCl_3 and BBr_3

BCl_3						BBr_3	
Final orbital	Term value[a]	Final orbital	Term value[b]	Final orbital	Term value[c]	Final orbital	Term value[b]
3p (a_2'')	2.19	2a_2''	5.1	2a_2''	5.1	2a_2''	5.4
4p (a_2'')	1.09	3a_1'	3.6	3a_1'	2.6	3a_1'	3.8
5p (a_2'')	0.67			4e′	1.5		
6p (a_2'')	0.45			3a_2''	~0.5[e]		
3p (e′)	2.01			5e′	~0.2[e]		
4p (e′)	1.04						
5p (e′)	0.64						
6p (e′)	0.43						
3d	~1.5[d]						
4d	0.85						
5d	0.54						
6d	0.40						

[a] Present data.
[b] Planckaert et al. [20].
[c] Baeck and Bartlett [16].
[d] Estimated through use of the Rydberg formula.
[e] Estimated from the calculated orbital energies.

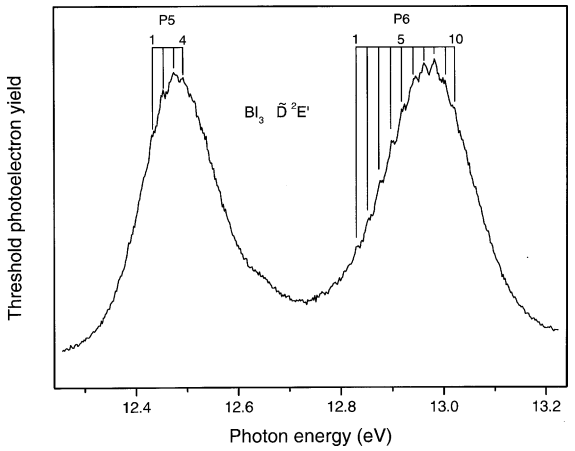

Fig. 13. TPES of BI_3 showing the band associated with the $\tilde{D}^2E'$ state.

calculated for BCl_3. The predicted results show reasonable agreement with the experimental data in the few cases where a comparison can be made. Term values deduced from their work are given in Table 5. The calculations indicate that the 5e′ orbital has an energy ~1.5 eV greater than that of the 4e′ orbital. Therefore we speculate that the $3e' \rightarrow 4e'$ and the $3e' \rightarrow 5e'$ excitations result in an enhancement of the transition probability into the near lying $np(e')$ Rydberg states and thereby account for the localised nature of the observed structure. Transitions involving excitation into orbitals of mixed Rydberg/valence character have been discussed previously in relation to the boron trihalides [5,6,11,12,16,18,20].

Theoretical studies [15,62–64] of elastic low-energy electron scattering by the boron trihalides have shown that shape resonances occur in the a_2'', e' and e″ channels within an energy range of a few eV above threshold. Unfortunately, similar work on the related photoionisation processes, which would help interpret the present data, has not been performed.

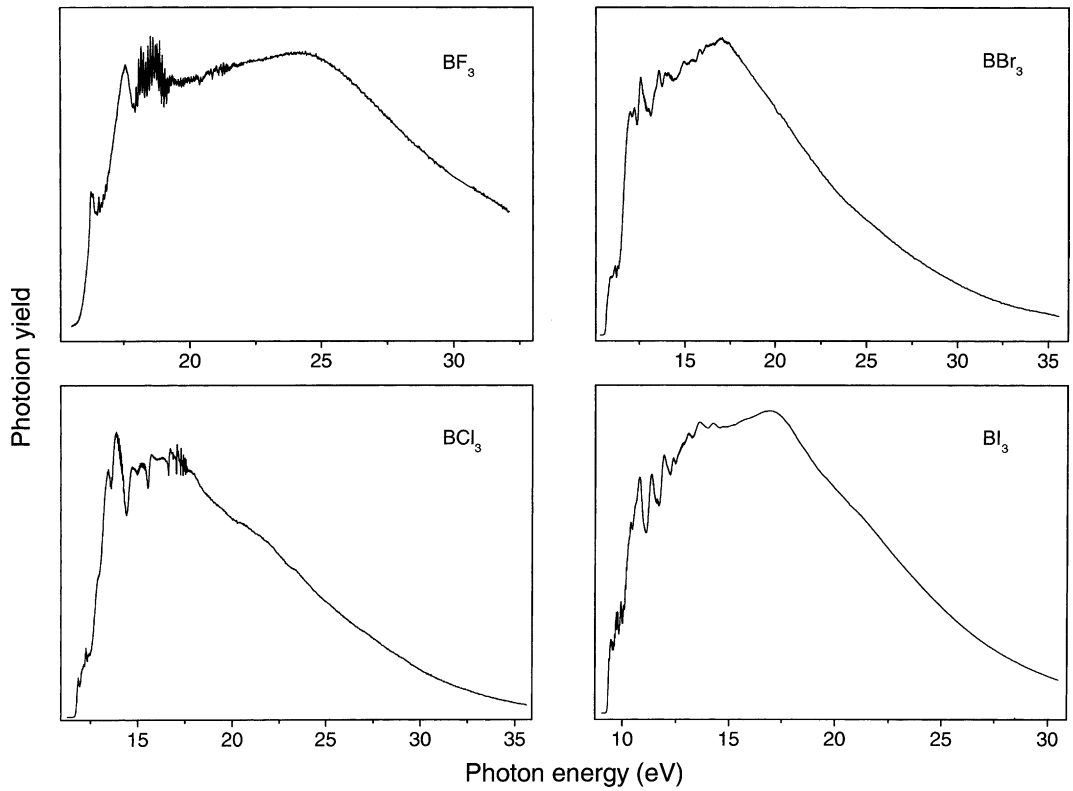

Fig. 14. The complete valence shell photoionisation yield curves of the boron trihalides.

3.2.2. Boron trifluoride

The photoionisation yield curve of BF_3 is shown in Figs. 15–17, and structure due to transitions into Rydberg or virtual valence orbitals can be observed up to ~21.5 eV. Some of these features appear in the photoabsorption spectrum recorded by Hagenow et al [18], but new structure is discernible in the ion yield curves, between 20.1 and 21.5 eV, which can be attributed to Rydberg series converging onto the $\tilde{E}^2A_1'$ state ionisation threshold. One of the surprising characteristics of the photoion yield curves is the apparent lack of structure attributable to Rydberg states associated with excitation from the $1a_2''$ orbital. In all four boron trihalides the $\tilde{C}^2A_2''$ state threshold photoelectron bands display an extended vibrational progression.

Hagenow et al. [18] have proposed that the structure appearing between 17.9 and 19.4 eV in the photoabsorption spectrum of BF_3 should be ascribed to two p-type and three d-type Rydberg series converging onto the $\tilde{D}^2E'$ state limit. To some extent we accept these assignments but we are not convinced that this apparently straightforward interpretation is completely supported by the experimental data. Even though our photoionisation yield curve was recorded using the same resolution (0.2 Å) as that used by Hagenow et al. [18], and appears to be of at least equivalent quality, it is difficult to distinguish many of the features identified by Hagenow et al. In D_{3h} symmetry, dipole selection rules allow the formation of $s(a_1')$, $p(e')$, $d(a_1')$, $d(e')$ and $d(e'')$ type Rydberg series following excitation from an orbital of e' symmetry. Hagenow et al. suggested that vibronic coupling was responsible for the observation of the dipole forbidden $p(a_2'')$ series.

The vibrational envelope of the strongest progression discernible in the HeI excited $\tilde{D}^2E'$ state photoelectron band of BF_3 reaches a maximum around $v_1^+ = 2$ [10,31]. Therefore we have

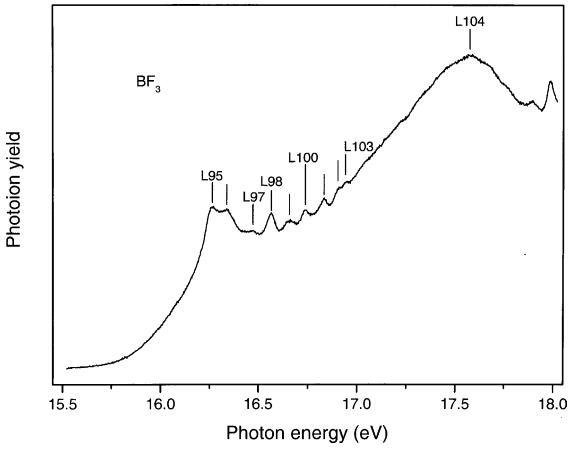

Fig. 15. Photoionisation yield curve of BF_3 showing the threshold region.

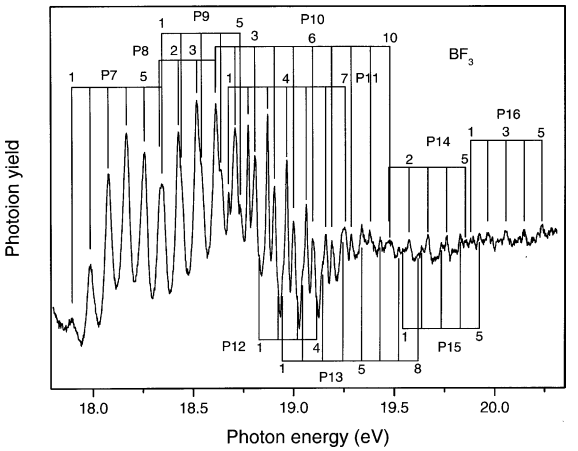

Fig. 16. Photoionisation yield curve of BF_3 showing vibrational progressions associated with Rydberg states belonging to series converging onto the $\tilde{D}^2E'$ state limit.

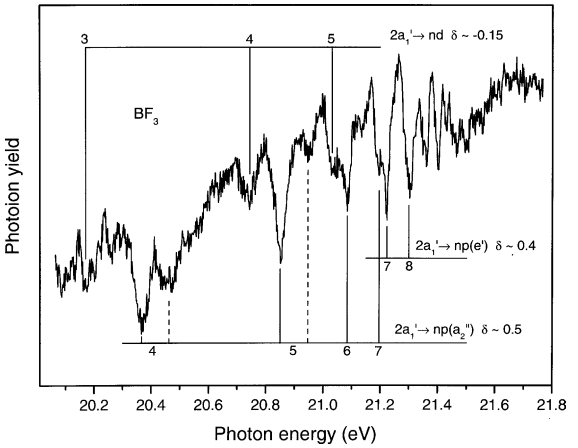

Fig. 17. Photoionisation yield curve of BF_3 showing Rydberg series due to excitation of the $2a_1'$ orbital.

attempted to identify vibrational progressions in the photoion spectrum between 17.8 and 20.2 eV by locating band maxima. This procedure should be more reliable than one using band onsets. The vibrational progressions (P7–P16) found in this way are given in Table 3 and marked in Fig. 16.

Based upon the term value and quantum defect it appears reasonable to assign P7 to the $2e' \rightarrow 3p(e')$ transition. All the peaks in this progression, occurring between ~17.8 and 18.4 eV, are fairly broad and symmetric. Hagenow et al. [18] have proposed that this region also contains contributions from the $2e' \rightarrow 3p(a_2'')$ transition but we are less confident about this interpretation. At energies above ~18.3 eV each main vibrational peak seems to be composed from at least two components. Our analysis suggests that the structure appearing between ~18.3 and 18.8 eV in the ion yield curve is mainly due to excitations from the 2e orbital into 3d Rydberg orbitals. For energies above 18.8 eV the structure becomes complex, with many overlapping vibrational progressions. The assignment of these progressions remains uncertain because we cannot distinguish regular Rydberg series. Hagenow et al. have proposed that all the features occurring between 17.9 and 19.4 eV should be attributed to five Rydberg series.

Excitation from the $2a_1'$ orbital results in at least one p-type and one d-type Rydberg series converging onto the $\tilde{E}^2A_1'$ state ionisation threshold, as indicated in Fig. 17. Only the lower members of these series can be identified with certainty because the structure in the ion yield curve becomes irregular at about 21.2 eV. Between 21.2 and 21.3 eV two strong features appear which could reasonably be ascribed to the $n = 7$ and 8 members of a second p-type Rydberg series. However, the other members of this series and the high-n members of the first two series cannot be identified even though the ion yield curve exhibits distinct structure up to about 21.5 eV. We speculate that an intervalence transition occurs in this energy region and leads to the regular features associated with the Rydberg states being perturbed.

In the TPES of BF_3, the vibrational progression occurring in the $\tilde{E}^2A_1'$ state band appears superimposed upon a continuum background intensity with an onset at ~21.4 eV. Yencha et al. [38] suggest that the continuum could be due to autoionisation from the shape resonantly enhanced $2e' \rightarrow 4e'$ transition. This seems unlikely because the e′ shape resonance has been predicted [13] and observed [35,37] to occur at ~26 eV in the 2e′ channel. The absorption features assigned by Hagenow et al. [18] to the $1e'' \rightarrow 2a_2''$, $2a_1' \rightarrow 2a_2''$ and $1a_2'' \rightarrow 3a_1'$ transitions result in term values of ~3.6–4.0 eV. Of the remaining dipole allowed intervalence transitions, only the $2a_1' \rightarrow 3a_2''$ excitation might occur in the relevant energy region. Evidently theoretical guidance will be required to achieve further progress.

3.2.3. Boron trichloride

In the energy region a few tenths of an eV above threshold, the photoion spectrum of BCl_3 (Fig. 18) displays four broad peaks which can be assigned to either an s-type or a d-type Rydberg series converging onto the $\tilde{B}^2E'$ state ionisation limit. As excitation from the 3e′ orbital in the other three boron trihalides results in an s-type series, we adopt the same notation for BCl_3 and assign the four peaks to the $n = 5$–8 members of an s-type Rydberg series with $\delta \sim 1.1$. Use of the Rydberg formula and the quantum defect derived from the present data allows the location of the preceding member ($n = 4$) to be estimated as 11.0 eV. This energy coincides with the position of the strongest feature discernible in the photoabsorption spectrum reported by Suto et al. [21].

Three vibrational progressions (P17–P19) can be observed between 13.4 and 14.4 eV superimposed upon two very broad peaks. In accordance with the discussion given in Section 3.2.1, all three progressions are assigned to Rydberg states belonging to series converging onto the $\tilde{D}^2E'$ state limit. Based upon the term values of ~2.0 eV for P17, and ~1.5 eV for P18 and P19, we ascribe P17 as being due to autoionisation from the $3p(e')$ Rydberg state, and the latter two progressions to a 3d Rydberg state. We also speculate that the $2e' \rightarrow 4e'$ transition lies in this energy region and may, in part, be responsible for the two broad peaks.

The average vibrational separations in progressions P17–P19 are 56, 53 and 52 meV, respectively, which indicates that the structure is due to excitation of the ν_1' mode. The offset between

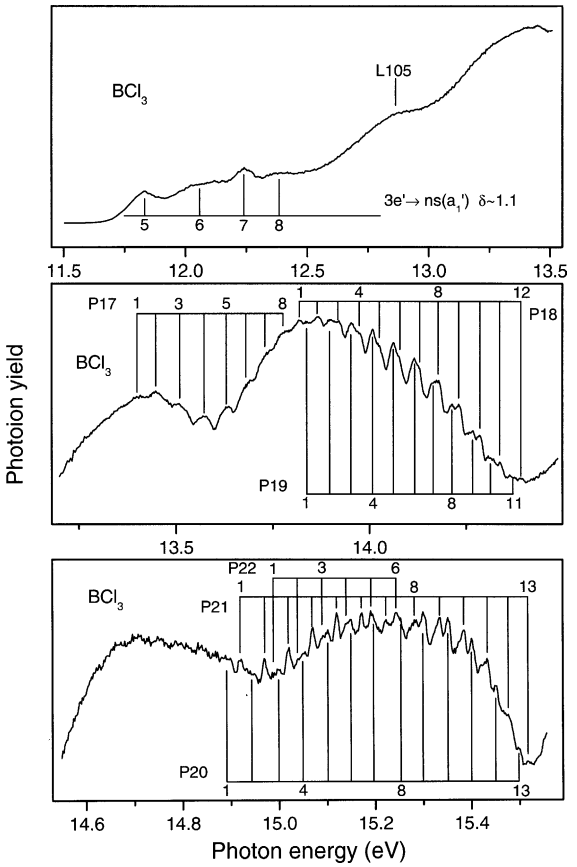

Fig. 18. Photoionisation yield curve of BCl_3. The vibrational progressions (P17–P22) are probably associated with Rydberg states belonging to series converging onto the $\tilde{D}^2E'$ state limit. The Rydberg states may be mixed with states due to intervalence transitions.

P18 and P19, although slightly irregular, is ~19–20 meV, and a comparison with the $\tilde{D}^2E'$ state TPES suggests that this offset corresponds to excitation of the ν_2' mode. Higher resolution might reveal additional features because the $\tilde{D}^2E'$ state threshold photoelectron band exhibits three vibrational progressions.

Three further progressions (P20–P22) occur in the ion yield curve between 14.8 and 15.6 eV (Fig. 18), again superimposed upon two very broad peaks. The vibrational spacing in each progression corresponds to excitation of the ν_1' mode, and the offsets of P21 and P22 with respect to P20 are 19 and 33 meV, respectively. These offsets may be associated with the ν_2' and ν_4' modes, respectively. Thus, the vibrational structure discernible in the photoion spectrum resembles that in the $\tilde{D}^2E'$ state threshold photoelectron band. The term value for the excited state responsible for this structure is ~0.3 eV, which suggests that these progressions may be associated with a high-n Rydberg state that is mixed with the valence state resulting from the $2e' \rightarrow 5e'$ transition. Alternatively, the structure may be due entirely to an excited valence state. Ishiguro et al. [5] have considered the mixing between Rydberg and valence states in their analysis of the B 1s excitation spectrum of BCl_3, and suggest that this perturbation leads to an irregular intensity distribution amongst members of a Rydberg series.

Excitation from the $2a_1'$ orbital results in three Rydberg series converging onto the $\tilde{E}^2A_1'$ state ionisation threshold, as shown in Fig. 19. Additional features, due to single excitation of the ν_1' mode, can be identified for several members of the $np(e')$ series and for the $n = 4$ member of the d series. The strong $np(a_2'')$ series has been observed previously by Creasey et al. [65] in the fluorescence excitation spectrum.

The photoabsorption spectrum of BCl_3 measured by Planckaert et al. [20] provides term values of ~5.1 and ~3.6 eV for valence shell excitations into the $2a_2''$ and $3a_1'$ orbitals, respectively. These values suggest that the only intervalence excita-

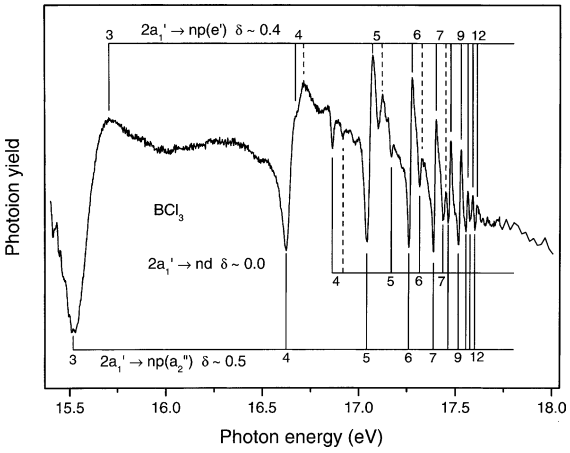

Fig. 19. Photoionisation yield curve of BCl_3 showing Rydberg series due to excitation of the $2a_1'$ orbital.

tions involving the $2a_2''$ or $3a_1'$ orbitals which could occur within the energy range relevant to the present study are the $2e' \rightarrow 3a_1'$ and $2a_1' \rightarrow 2a_2''$ transitions. It is conceivable that these transitions contribute to the broad features observed in the photoion spectrum between 11.7 and 13.0 eV. Hagenow et al. [18] attributed a broad feature in the photoabsorption spectrum of BF_3 to the $2a_1' \rightarrow 2a_2''$ transition.

3.2.4. Boron tribromide

Between 10.9 and 11.6 eV the photoionisation yield curve of BBr_3, shown in Fig. 20, displays structure that can be attributed to autoionisation from two Rydberg series converging onto the ionisation limit for the $E_{3/2}$ component of the $\tilde{B}^2E'$ state. One series, having $\delta \sim 0.5$, clearly corresponds to excitation from the 3e′ orbital into p-type Rydberg orbitals. Planckaert et al. [20] have observed the $n = 3$ and 4 members at 9.732 and 10.619 eV, respectively. The other series could be designated either as ns with $\delta \sim 1.0$ or as nd with $\delta \sim 0.0$. Both are dipole allowed transitions. Planckaert et al. [20] have assigned a feature occurring at 10.192 eV in the photoabsorption spectrum to the $3e' \rightarrow 4s$ excitation. Therefore, we follow this notation and associate the peak at 10.901 eV with the $3e' \rightarrow 5s$ transition.

Vibrational progressions can be observed in two regions of the ion yield curve, as shown in Figs. 21 and 22. The first region occurs between 12.5 and 13.2 eV, and contains at least three progressions (P23–P25), each involving the ν_1' mode. The offset between P23 and P24 is ~9 meV, which corresponds to a single excitation of the ν_2' mode. The vibrational progressions are superimposed upon a broad asymmetric peak which may, in part, be due to the $2e' \rightarrow 4e'$ transition. It appears that the structure between 12.5 and 13.2 eV should be assigned to autoionisation from two Rydberg states formed through excitation of the 2e′ orbital. However, it is not clear if the two states correspond to the $2e' \rightarrow 3p$ and $2e' \rightarrow 3d$ transitions, or whether both excitations occur into 3d orbitals.

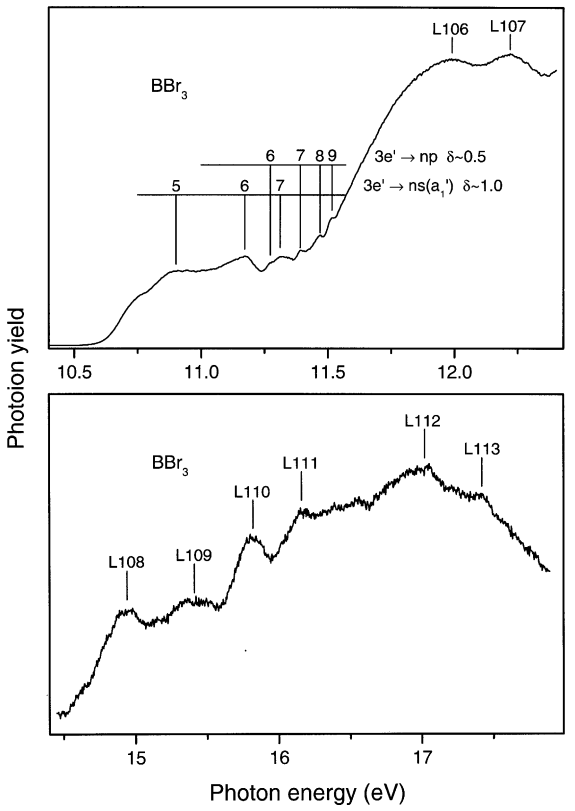

Fig. 20. Photoionisation yield curve of BBr_3 showing the threshold region, and the features associated with the inner valence orbitals.

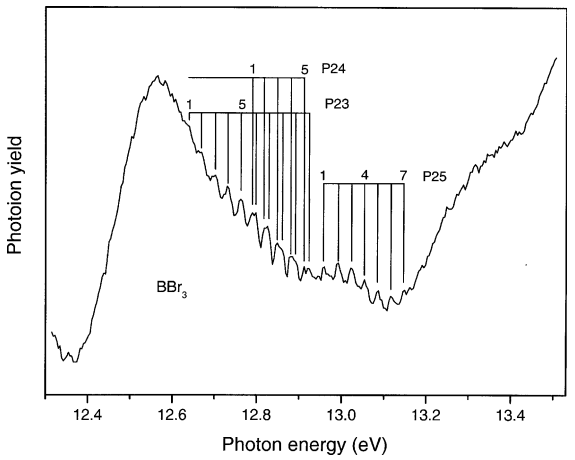

Fig. 21. Photoionisation yield curve of BBr_3. The vibrational progressions (P23–P25) are probably associated with Rydberg states belonging to series converging onto the $\tilde{D}^2E'$ state limit. The Rydberg states may be mixed with states due to intervalence transitions.

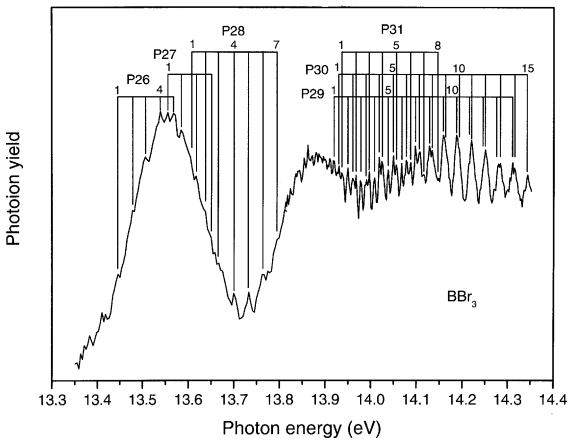

Fig. 22. Photoionisation yield curve of BBr_3. Possible assignments of the structure are discussed in the text.

The second region exhibiting vibrational structure occurs between 13.4 and 14.5 eV, and, although some of the features are weak, several progressions can be identified. All the progressions involve excitation of the ν_1' mode. We assign the vibrational structure (P26–P28) occurring between 13.4 and ~13.8 eV to the Rydberg states associated with the $2e' \rightarrow 4p$ and the $2e' \rightarrow 4d$ transitions. Progressions P31 and P29 are offset from P30 by intervals of 8 and 19 meV, and these energies are attributed to the ν_2' and the ν_4' modes, respectively. The designation of the states resulting in progressions P29–P31 is difficult. It appears that these progressions are due either to transitions into high-n Rydberg states or to intervalence excitations. It is noticeable that the progressions are superimposed upon two broad peaks, one of which may correspond to the $2e' \rightarrow 5e'$ transition. Many of the features discernible in the ion yield curve between 14.1 and 14.5 eV coincide with peaks in the TPES.

Between 14.6 and 17.5 eV the photoion spectrum (Fig. 20) displays several broad features, most of which do not correlate with structure in the TPES. It is not evident that any of the features occurring below 16.7 eV can be attributed to Rydberg series converging onto the $\tilde{E}^2A_1'$ state ionisation limit.

The photoabsorption spectrum of BBr_3 recorded by Planckaert et al. [20] allows term values of 5.4 and 3.8 eV to be derived for valence shell excitations into the $2a_2''$ and $3a_1'$ orbitals, respectively. These term values suggest that the $2e' \rightarrow 3a_1'$ and $2a_1' \rightarrow 2a_2''$ transitions may contribute to the photoion yield close to threshold. Excitation into the $3a_2''$ orbital is allowed from both the $1e''$ and $2a_1'$ orbitals. Although the energy of the $1e'' \rightarrow 3a_2''$ transition may fall below the ionisation threshold, that of the $2a_1' \rightarrow 3a_2''$ transition should occur in an energy region relevant to the present study. Therefore it is conceivable that some of the broad structure which remains unassigned may be ascribed to the $2a_1' \rightarrow 3a_2''$ transition.

3.2.5. Boron triiodide

Between the ionisation threshold and 10.3 eV the photoionisation yield curve of BI_3, shown in Fig. 23, displays structure due to autoionising

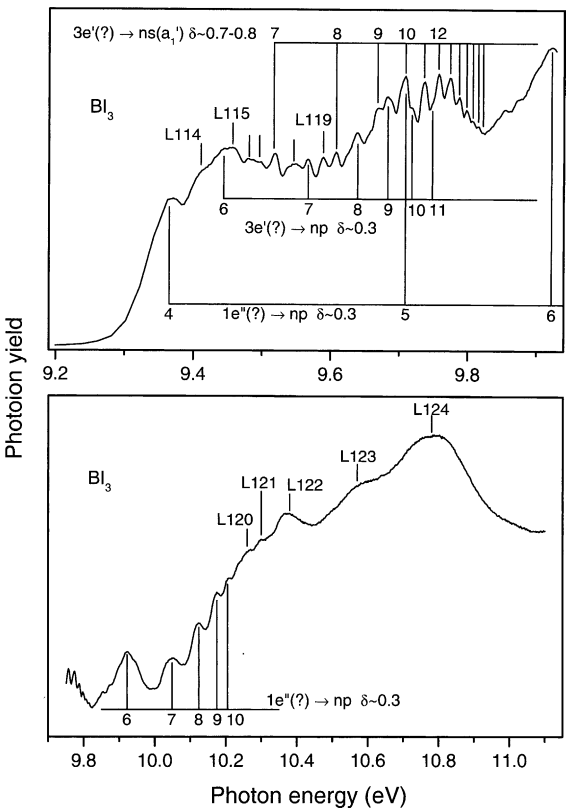

Fig. 23. Photoionisation yield curve of BI_3 showing Rydberg series due to excitation of the 3e′ or the 1e″ orbital.

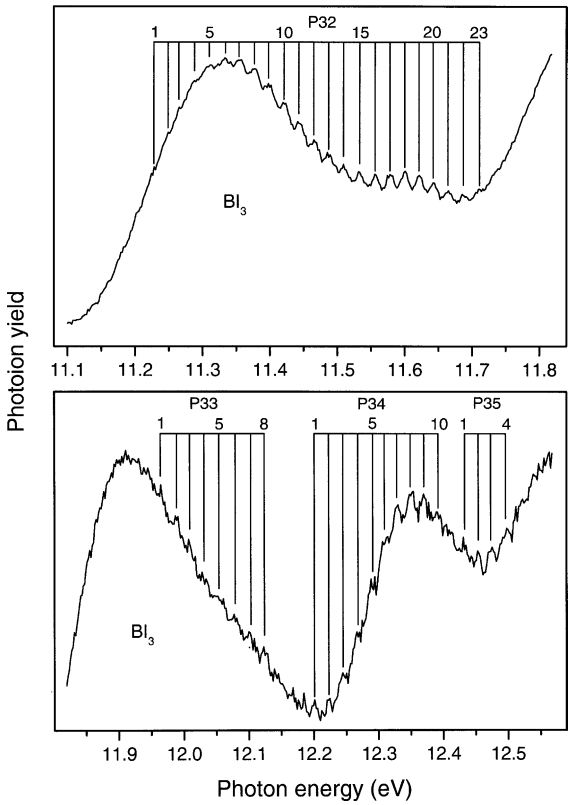

Fig. 24. Photoionisation yield curve of BI_3. Possible assignments of the structure are discussed in the text.

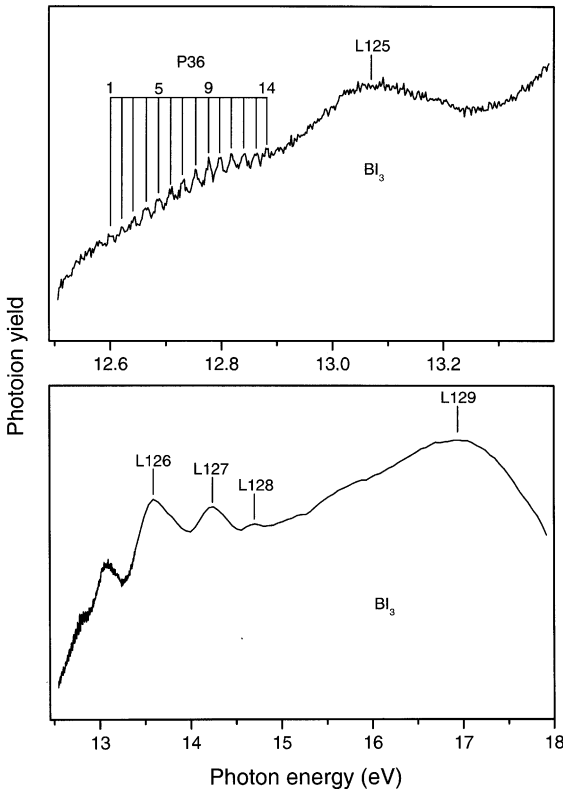

Fig. 25. Photoionisation yield curve of BI_3. Possible assignments of the structure are discussed in the text.

Rydberg states. Most of the peaks occurring between 9.4 and 9.85 eV can be attributed to two Rydberg series converging onto the $E_{5/2}$ component of the $\tilde{A}^2E'$ state. Quantum defects of 0.3 and 0.7–0.8 are obtained for these two series, which suggests that the series should be designated as p-type and s-type, respectively. Another p-type Rydberg series, with $\delta \sim 0.3$, occurs between 9.9 and 10.3 eV and converges onto the ionisation limit at 10.351 eV.

At higher energies the ion yield curve (Figs. 24 and 25) reveals extended vibrational progressions in three energy regions, and it is noticeable that in each case the structure is superimposed upon broad features attributable to intervalence transitions. The vibrational structure in the ion yield curve is similar to that in the $\tilde{D}^2E'$ state threshold photoelectron band, and is therefore assigned to Rydberg states belonging to series converging onto this limit. The energy separation between the $E_{5/2}$ and $E_{3/2}$ spin–orbit components of the $\tilde{D}^2E'$ state is ~0.5 eV, and this results in an additional uncertainty in the term value analysis. Nevertheless, it appears that the term value for the structure (P32) occurring between 11.2 and 11.7 eV is too small for these features to be attributed to the $2e' \rightarrow 3p$ transition. The vibrational spacing indicates that the ν_1' mode is being excited. The structure appears to exhibit two maxima, one at ~11.4 eV and the other at ~11.6 eV. Therefore we tentatively propose that transitions into at least one, and probably two, 3d Rydberg states occur in this energy region.

The second energy range in which the photoion spectrum exhibits vibrational structure (P33-P35) occurs between 11.9 and 12.5 eV. Again, this structure is superimposed upon broad peaks due to intervalence transitions. The vibrational pro-

gressions probably result from excitations into more than one state, and we tentatively associate the features with the $2e' \rightarrow 4p$, 5p and 4d transitions. However, we note that many of the peaks observed in the ion yield curve between 12.4 and 12.5 eV coincide with structure in the $E_{5/2}$ spin–orbit component of the $\tilde{D}^2E'$ state threshold photoelectron band.

Finally, a short progression (P36), involving the v_1' mode, appears in the photoion spectrum between 12.6 and 12.9 eV. This energy range coincides with the minimum between the two peaks associated with the $E_{5/2}$ and $E_{3/2}$ components of the $\tilde{D}^2E'$ state threshold photoelectron band.

Several broad peaks appear in the photoionisation yield curve between 13.5 and 17.5 eV, and are shown in Fig. 25. However, as was the case with BBr_3, it seems that none of these peaks belongs to a Rydberg series converging onto the $\tilde{E}^2A_1'$ state limit.

4. Summary

The valence shell threshold photoelectron spectra of the boron trihalides have been recorded and these have enabled an almost complete set of ionic vibrational energies (Table 6) to be obtained. The increasing influence of spin–orbit coupling in the heavier trihalides is revealed in the photoelectron bands associated with ionisation from degenerate orbitals. Three vibrational progressions, each involving excitation of the v_1^+ mode, have been observed in the $\tilde{D}^2E'$ state threshold photoelectron bands of BF_3, BCl_3 and BBr_3. The second and third progressions are offset from the first by energy intervals which have been attributed, tentatively, to a single quantum of the v_2^+ and v_4^+ modes, respectively. The assignment of the smaller of these offsets to the v_2^+ mode remains uncertain because the mechanism through which this vibrational mode becomes excited in the $\tilde{D}^2E'$ state has not been established. Energy considerations suggest that hot band excitations cannot account for the observed spacing. Tables 1 and 6 indicate that the energies of the v_1^+ and v_4^+ modes are reduced only slightly in comparison with the corresponding energies in the molecular ground state. On the other hand, the energy of v_3^+ is greater than that of v_3. If it is assumed that the smaller offset does correspond to a single excitation of v_2^+, then the vibrational energy of this mode is reduced significantly from its molecular ground state value. For BF_3, Jacox and Thompson [44] give an energy of 16.0 meV for the v_2^+ mode which is substantially different to the value attributed to this mode in the present study. This unsatisfactory situation requires theoretical guidance, and also a consideration of matrix effects on the ion structure.

In addition to the threshold photoelectron bands associated with direct ionisation, features have been observed due to autoionisation from Rydberg or valence excited states. In most cases the effect of this resonant process can be seen more clearly in the photoionisation yield curves. The interpretation of the TPES of BI_3 has been hampered by the uncertainty surrounding the electronic configuration.

The valence shell photoionisation yield curves have revealed some, generally rather weak, vibrational progressions and demonstrate that intervalence transitions play a major role in this energy

Table 6
Summary of the energies of the four normal modes of vibration in the boron trihalide cations

Normal mode	Vibrational energy (meV)			
	BF_3	BCl_3	BBr_3	BI_3
v_1^+	96	53	32	22
v_2^+	32	19	8	
v_3^+	253	132		
v_4^+	56	30	18	

The energies of the v_1^+, v_2^+, v_3^+ and v_4^+ modes were obtained from vibrational progressions occurring in the $\tilde{C}^2A_2''$, $\tilde{D}^2E'$, $\tilde{E}^2A_1'$ and $\tilde{D}^2E'$ state threshold photoelectron bands, respectively.

region. Several new Rydberg series have been observed and some of these have been assigned. Excitation from the 3e′ orbital gives rise to an s-type Rydberg series in each of the boron trihalides, and in BBr_3 and BI_3 a p-type series also occurs. It appears that many of the vibrational progressions should be associated with states resulting from excitation of the 2e′ orbital. In some Rydberg series the intensity distribution amongst the members seems irregular and this perturbation may be caused by mixing between Rydberg states and valence excited states. Some of the vibrational progressions occur within a few tenths of an eV of the ionisation limit to which the Rydberg state is converging. All the photoionisation spectra exhibit prominent broad features associated with intervalence transitions but for the most part these remain unassigned. Progress on this issue requires theoretical predictions for intervalence transition energies.

Acknowledgements

We thank the Engineering and Physical Sciences Research Council for financial support.

References

[1] V.A. Fomichev, Sov. Phys. Solid State 9 (1968) 2496.
[2] V.A. Fomichev, J. Struct. Chem. 11 (1970) 810.
[3] W. Hayes, F.C. Brown, J. Phys. B 4 (1971) L85.
[4] T.M. Zimkina, A.S. Vinogradov, Bull. Acad. Sci. USSR 36 (1972) 229.
[5] E. Ishiguro, S. Iwata, Y. Suzuki, A. Mikuni, T. Sasaki, J. Phys. B 15 (1982) 1841.
[6] W.H.E. Schwarz, L. Mensching, K.H. Hallmeier, R. Szargan, Chem. Phys. 82 (1983) 57.
[7] V.I. Nefedov, J. Struct. Chem. 11 (1970) 272.
[8] J.L. Dehmer, J. Chem. Phys. 56 (1972) 4496.
[9] H. Biehl, D.M. Smith, R.P. Tuckett, K.R. Yoxall, H. Baumgärtel, H.W. Jochims, U. Rokland, Mol. Phys. 87 (1996) 1199.
[10] L.G. Shpinkova, D.M.P. Holland, D.A. Shaw, Mol. Phys. 96 (1999) 323.
[11] D. Goutier, L.A. Burnelle, Chem. Phys. Lett. 18 (1973) 460.
[12] B. Cadioli, U. Pincelli, E. Tosatti, U. Fano, J.L. Dehmer, Chem. Phys. Lett. 17 (1972) 15.
[13] J.R. Swanson, D. Dill, J.L. Dehmer, J. Chem. Phys. 75 (1981) 619.
[14] F.A. Gianturco, E. Semprini, F. Stefani, Il Nuovo Cimento 2D (1983) 687.
[15] J.A. Tossell, J.H. Moore, J.K. Olthoff, Int. J. Quantum Chem. 29 (1986) 1117.
[16] K.K. Baeck, R.J. Bartlett, J. Chem. Phys. 106 (1997) 4606.
[17] H.J. Maria, J.R. McDonald, S.P. McGlynn, J. Am. Chem. Soc. 95 (1973) 1050.
[18] G. Hagenow, K. Hottmann, H.W. Jochims, H. Baumgärtel, Chem. Phys. 137 (1989) 287.
[19] M. Suto, C. Ye, L.C. Lee, Phys. Rev. A 42 (1990) 424.
[20] A.A. Planckaert, P. Sauvageau, C. Sandorfy, Chem. Phys. Lett. 20 (1973) 170.
[21] M. Suto, C. Ye, J.C. Han, L.C. Lee, J. Chem. Phys. 89 (1988) 6653.
[22] L.C. Lee, J.C. Han, M. Suto, J. Chem. Phys. 91 (1989) 2036.
[23] V.H. Dibeler, S.K. Liston, Inorg. Chem. 7 (1968) 1742.
[24] V.H. Dibeler, J.A. Walker, Inorg. Chem. 8 (1969) 50.
[25] R.J. Boyd, D.C. Frost, Chem. Phys. Lett. 1 (1968) 649.
[26] P.J. Bassett, D.R. Lloyd, J. Chem. Soc. Chem. Commun. (1970) 36.
[27] A.W. Potts, H.J. Lempka, D.G. Streets, W.C. Price, Philos. Trans. R. Soc. Lond. A 268 (1970) 59.
[28] P.J. Bassett, D.R. Lloyd, J. Chem. Soc. A (1971) 1551.
[29] G.H. King, S.S. Krishnamurthy, M.F. Lappert, J.B. Pedley, Discuss. Faraday Soc. 54 (1972) 70.
[30] K. Kimura, S. Katsumata, T. Achiba, T. Yamazaki, S. Iwata, Handbook of HeI Photoelectron Spectra of Fundamental Organic Molecules, Scientific Societies Press, Tokyo, 1981.
[31] G. Hagenow, K. Hottmann, H. Baumgärtel, Chem. Phys. Lett. 164 (1989) 395.
[32] C.S. Sreekanth, C.Y. Mok, H.H. Huang, K.L. Tan, J. Electron Spectrosc. Relat. Phenom. 58 (1992) 129.
[33] L. Åsbrink, A. Svensson, W. von Niessen, G. Bieri, J. Electron Spectrosc. Relat. Phenom. 24 (1981) 293.
[34] C.F. Batten, J.A. Taylor, B.P. Tsai, G.G. Meisels, J. Chem. Phys. 69 (1978) 2547.
[35] J.L. Dehmer, A.C. Parr, S.H. Southworth, D.M.P. Holland, Phys. Rev. A 30 (1984) 1783.
[36] H. Biehl, K.J. Boyle, D.M. Smith, R.P. Tuckett, K.R. Yoxall, K. Codling, P.A. Hatherly, M. Stankiewicz, J. Chem. Soc. Faraday Trans. 92 (1996) 185.
[37] D.M.P. Holland, M.A. MacDonald, M.A. Hayes, L. Karlsson, B. Wannberg, Chem. Phys. 226 (1998) 351.
[38] A.J. Yencha, M.C.A. Lopes, G.C. King, Chem. Phys. 279 (2002) 55.
[39] T.E.H. Walker, J.A. Horsley, Mol. Phys. 21 (1971) 939.
[40] E. Haller, H. Köppel, L.S. Cederbaum, G. Bieri, W. von Niessen, Chem. Phys. Lett. 85 (1982) 12.
[41] E. Haller, H. Köppel, L.S. Cederbaum, W. von Niessen, G. Bieri, J. Chem. Phys. 78 (1983) 1359.
[42] R.N. Dixon, quoted as private communication in [9].
[43] J.H. Miller, L. Andrews, J. Am. Chem. Soc. 102 (1980) 4900.

[44] M.E. Jacox, W.E. Thompson, J. Chem. Phys. 102 (1995) 4747.
[45] M.E. Jacox, K.K. Irikura, W.E. Thompson, J. Chem. Phys. 104 (1996) 8871.
[46] M.W. Chase, C.A. Davies, J.R. Downey, D.J. Frurip, R.A. McDonald, A.N. Syverud, J. Phys. Chem. Ref. Data 14 (1) (1985).
[47] D.M.P. Holland, D.A. Shaw, I. Sumner, M.A. Hayes, R.A. Mackie, B. Wannberg, L.G. Shpinkova, E.E. Rennie, L. Cooper, C.A.F. Johnson, J.E. Parker, Nucl. Instrum. Methods B 179 (2001) 436.
[48] D.M.P. Holland, J.B. West, A.A. MacDowell, I.H. Munro, A.G. Beckett, Nucl. Instrum. Methods B 44 (1989) 233.
[49] G. Herzberg, Electronic Spectra and Electronic Structure of Polyatomic Molecules, vol. 3, Van Nostrand Reinhold, New York, 1966.
[50] J.H.D. Eland, Photoelectron Spectroscopy, Butterworths, London, 1974.
[51] L.S. Cederbaum, W. Domcke, J. Schirmer, W. von Niessen, Adv. Chem. Phys. 65 (1986) 115.
[52] E. Weigold, Y. Zheng, W. von Niessen, Chem. Phys. 184 (1994) 13.
[53] L. Cooper, L.G. Shpinkova, D.M.P. Holland, D.A. Shaw, Chem. Phys. 270 (2001) 363.
[54] H. Biehl, J.C. Creasey, D.M. Smith, R.P. Tuckett, K.R. Yoxall, H. Baumgärtel, H.W. Jochims, U. Rokland, J. Chem. Soc. Faraday Trans. 91 (1995) 3073.
[55] N. Kaltsoyannis, S.D. Price, Chem. Phys. Lett. 313 (1999) 679.
[56] T.M. Zimkina, V.A. Fomichev, Sov. Phys. Dokl. 11 (1967) 726.
[57] R.E. LaVilla, J. Chem. Phys. 57 (1972) 899.
[58] A.S. Vinogradov, T.M. Zimkina, Opt. Spectrosc. 32 (1972) 17.
[59] D. Blechschmidt, R. Haensel, E.E. Koch, U. Nielsen, T. Sagawa, Chem. Phys. Lett. 14 (1972) 33.
[60] K.H. Sze, C.E. Brion, Chem. Phys. 140 (1990) 439.
[61] D.M.P. Holland, D.A. Shaw, A. Hopkirk, M.A. MacDonald, S.M. McSweeney, J. Phys. B 25 (1992) 4823.
[62] W.A. Isaacs, C.W. McCurdy, T.N. Rescigno, Phys. Rev. A 58 (1998) 2881.
[63] M.H.F. Bettega, Phys. Rev. A 61 (2000) 042703.
[64] M.H.F. Bettega, Phys. Rev. A 62 (2000) 024701.
[65] J.C. Creasey, P.A. Hatherly, I.R. Lambert, R.P. Tuckett, Mol. Phys. 79 (1993) 413.